MYC Induces a Hybrid Energetics Program Early in Cell Reprogramming

Javier Prieto,[1,7] Arnold Y. Seo,[2,8] Marian León,[1,8] Fulvio Santacatterina,[3] Laura Torresano,[3]
Martina Palomino-Schätzlein,[4,6] Karen Giménez,[1] Azahara Vallet-Sánchez,[1] Xavier Ponsoda,[1]
Antonio Pineda-Lucena,[4,6] José M. Cuezva,[3] Jennifer Lippincott-Schwartz,[2] and Josema Torres[1,5,*]

[1]Dpto. Biología Celular, Biología Funcional y Antropología Física, Universidad de Valencia, 46100 Burjassot, Spain
[2]Janelia Research Campus, Howard Hughes Medical Institute (HHMI), Ashburn, VA 20147, USA
[3]Dpto. Biología Molecular, Centro de Biología Molecular Severo Ochoa, Centro de Investigación Biomédica en Red de Enfermedades Raras CIBERER-ISCIII,
Instituto de Investigación Hospital 12 de Octubre, Universidad Autónoma de Madrid, 28049 Madrid, Spain
[4]Structural Biochemistry Laboratory, Centro de Investigación Príncipe Felipe, 46012 Valencia, Spain
[5]Instituto de Investigación Sanitaria INCLIVA, 46010 Valencia, Spain
[6]Joint Research Unit in Clinical Metabolomics CIPF/IIS La Fe, Drug Discovery Unit, IIS La Fe, 46026 Valencia, Spain
[7]Present address: Gene Expression Laboratory, Salk Institute for Biological Studies, 10010 North Torrey Pines Road, La Jolla, CA 92037, USA
[8]These authors contributed equally
*Correspondence: josema.torres@uv.es
 https://doi.org/10.1016/j.stemcr.2018.10.018

SUMMARY

Cell reprogramming is thought to be associated with a full metabolic switch from an oxidative- to a glycolytic-based metabolism. However, neither the dynamics nor the factors controlling this metabolic switch are fully understood. By using cellular, biochemical, protein array, metabolomic, and respirometry analyses, we found that c-MYC establishes a robust bivalent energetics program early in cell reprogramming. Cells prone to undergo reprogramming exhibit high mitochondrial membrane potential and display a hybrid metabolism. We conclude that MYC proteins orchestrate a rewiring of somatic cell metabolism early in cell reprogramming, whereby somatic cells acquire the phenotypic plasticity necessary for their transition to pluripotency in response to either intrinsic or external cues.

INTRODUCTION

Somatic cells can be reprogrammed to pluripotency by forced expression of OCT4, SOX2, KLF4, and c-MYC (OSKM hereafter) (Takahashi and Yamanaka, 2006). Genome-wide and proteomic studies have shown that OSKM-induced reprogramming is a multi-step process characterized by two waves of gene expression and proteome resetting (Buganim et al., 2012; Hansson et al., 2012; Polo et al., 2012). During the first wave, there is a stochastic activation of genes controlling cell proliferation, metabolism, and cytoskeletal reorganization, and a downregulation of somatic gene expression signatures. A transient phase then follows, whereby a reduced group of cells upregulates early stem cell markers. In the second wave, the robust upregulation of core pluripotency circuitry genes, silencing of exogenous reprogramming factors, and the complete resetting of somatic epigenetic marks takes place, leading to the definitive stabilization of the pluripotent state.

MYC family members of transcription factors play central roles in the regulation of a wide range of cellular processes by controlling the expression of discrete groups of genes directly or in a secondary response fashion (Dang, 2016; Kress et al., 2015). Although its overexpression is dispensable for the process, the presence of c-MYC in the cocktail is favorable for cell reprogramming (Nakagawa et al., 2008; Wernig et al., 2008). Paradoxically, while sustained high levels of c-MYC are beneficial at early stages,

elevated expression of this proto-oncogene at later stages is detrimental for cell reprogramming (Sridharan et al., 2009; Zhuang et al., 2018).

A hallmark of cell reprogramming is the metabolic switch undertaken by somatic cells from an oxidative phosphorylation (OXPHOS)-based metabolism to a metabolic state substantiated on aerobic glycolysis (Folmes et al., 2011). As this postulation is based on the comparison between the somatic and pluripotent endpoint metabolic profiles, neither the dynamics nor the factors orchestrating this metabolic switch during the reprogramming process are completely understood. Here we show that c-MYC plays a central role in modulating metabolic pathways to favor somatic cell fate change.

RESULTS

Cell Reprogramming-Induced Mitochondrial Fission Is c-MYC Dependent

Cell reprogramming experiments in the presence or absence of exogenous c-MYC (Nakagawa et al., 2008; Wernig et al., 2008) have nourished the perception of a non-essential role in the reprogramming process for the *MYC* gene family. As these experiments have only tested the overexpression effect of *MYC* genes, an important role for this gene family in the reprogramming process may have been overlooked. We therefore sought to investigate the role of endogenous MYC activity in somatic cell
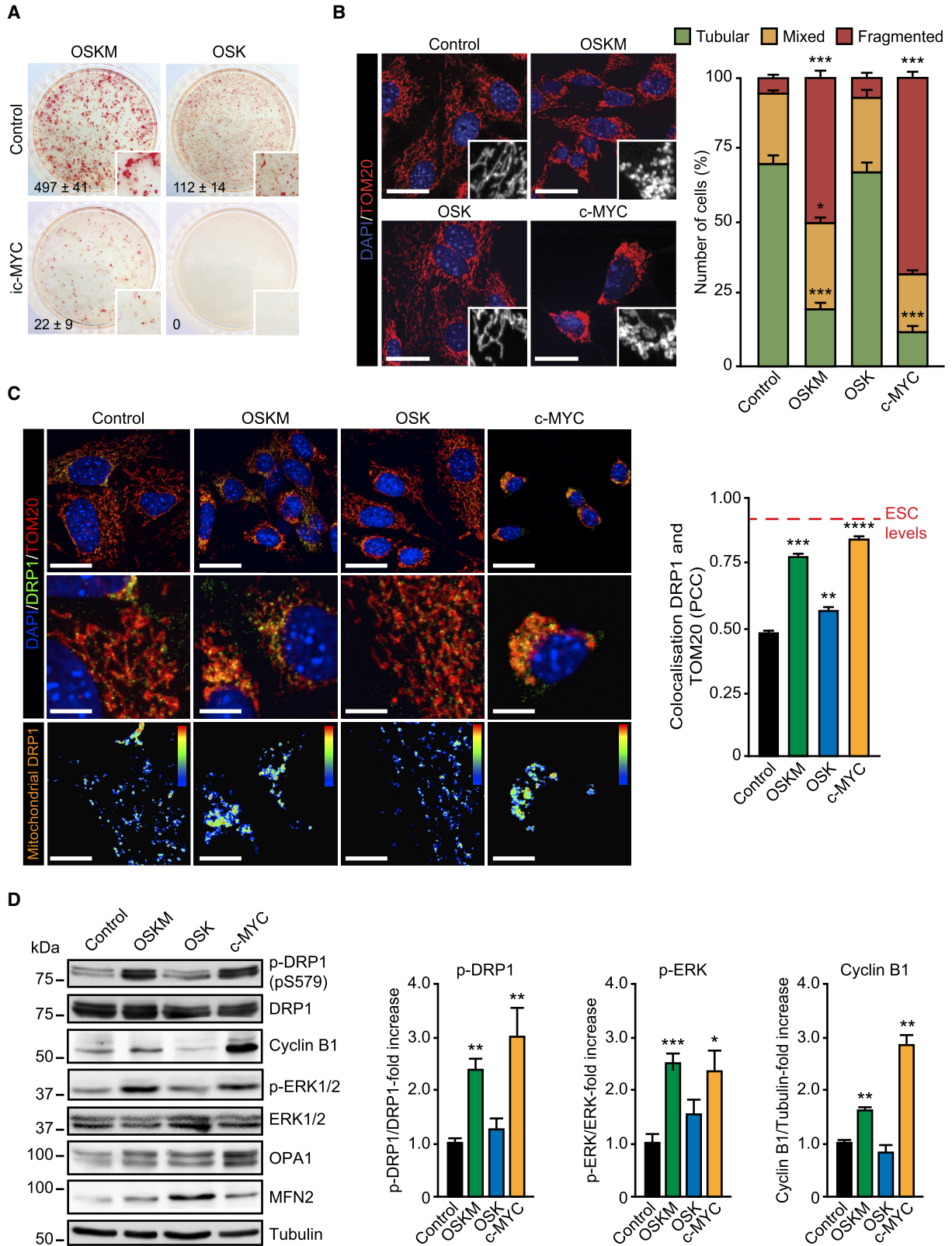
(legend on next page)

reprogramming. For this, we conducted cell reprogramming experiments in the presence or absence of the MYC inhibitor 10058-F4 (ic-MYC), known to impair endogenous MYC biological activity (Scognamiglio et al., 2016). Cell reprogramming, assessed by scoring the number of alkaline phosphatase (AP)-positive colonies, induced by overexpression of OSKM in mouse embryonic fibroblasts (MEFs) was greatly impaired in the presence of the MYC inhibitor (Figure 1A). Remarkably, cell reprogramming in the absence of exogenous c-MYC, induced by ectopic expression of OCT4, SOX2, and KLF4 (OSK hereafter), was completely abolished by treatment of the cells with the MYC inhibitor and no AP-positive colonies were detected (Figure 1A). These results indicate that endogenous MYC activity is necessary for somatic cell reprogramming.

ERK1/2-mediated mitochondrial fission is a necessary event for OSKM-induced cell reprogramming (Prieto et al., 2016a, 2016b). We next investigated the role of MYC in OSKM-induced mitochondrial fission early in cell reprogramming. OSK cells transduced for 4 days showed identical mitochondrial morphology to that of controls whereas ∼50% of OSKM-transduced cells displayed fragmented mitochondria (Figure 1B). Remarkably, ∼70% of the cells presented fragmented mitochondria in c-MYC-expressing cells (Figure 1B). OSKM or c-MYC induced a robust recruitment of dynamin-related protein 1 (DRP1) to mitochondria, whereas the association of DRP1 with these organelles augmented only slightly by OSK (Figure 1C). Accordingly, and compared with control and OSK-expressing MEFs, ERK1/2 and DRP1-S579 phosphorylation were increased about 3-fold by OSKM- or c-MYC (Figure 1D), indicating that OSKM-induced mitochondrial fission is

c-MYC dependent. Also, we observed an increase in cyclin B1 protein in OSKM- and c-MYC-expressing cells (Figure 1D and see below).

Treatment of c-MYC-expressing cells with a MEK1/2 inhibitor decreased both DRP1-S579 phosphorylation and mitochondrial fission (Figures S1A and S1B, respectively). Interestingly, reduction of c-MYC-induced mitochondrial fission by the MEK1/2 inhibitor was rescued by co-expression of DRP1-S579D phosphomimetic mutation, but not by the wild-type form of the dynamin (Figure S1C). Activation of ERK signaling early in reprogramming is associated with a decrease in *Dusp6* gene expression (Prieto et al., 2016a), the major cytosolic ERK1/2-phosphatase (Kidger and Keyse, 2016; Ríos et al., 2014). While expression of this phosphatase decreased by ∼20% in c-MYC- and OSK-expressing cells, OSKM expression led to ∼40% reduction in *Dusp6* mRNA levels (Figure S1D), suggesting a cooperation between the four factors in reducing the expression of this phosphatase. In addition to *Dusp6*, other phosphatases known to target ERK1/2 (Ríos et al., 2014) were also downregulated in response to OSKM, OSK, or c-MYC expression (Figure S1D). Altogether, our results indicate that OSKM-induced DRP1 activation and mitochondrial fission are c-MYC dependent.

Overexpression of c-MYC triggers cell-cycle progression (Figure S2A), a cell reprogramming hallmark. We found that this rise in cell proliferation by either OSKM or c-MYC was associated with an increase in *Ccnb1* and *Ccnb2* gene transcripts (Figure S2B), cyclin B1 protein, and DRP1-S579 phosphorylation (Figures 1D and S2C). Interestingly, cyclin B1 is a key component of the CDK1 complex (Bretones et al., 2015). CDK1 phosphorylates

Figure 1. Role of c-MYC in Cell Reprogramming-Induced Mitochondrial Fission

(A) Representative bright-field images after alkaline phosphatase (AP) staining of plates containing MEFs after 25 days of either OSK (right panels) or OSKM (left panels) retroviral delivery in the presence of DMSO (control) or the MYC inhibitor 10058-F4 (ic-MYC, 10 μM). Inset shows a magnification of a selected area from the AP-stained plates. Data on the bottom left-hand side of the pictures represent the mean ± SEM of three independent experiments.

(B) MEFs were mock-infected (control) or transduced with the indicated factors. At day 4 post transduction, cells were fixed and mitochondrial morphology assessed by immunofluorescence. Left panels: representative confocal images of MEFs stained with anti-TOM20 antibodies (red) before (control) or after expressing the indicated factors. Inset shows a black-and-white magnification of the pictures. DAPI (blue) was used as a nuclear counterstaining. Graph on the right shows the quantification of the different mitochondrial morphologies.

(C) Representative confocal images of MEFs before (Control) or 4 days after OSKM, OSK, or c-MYC expression stained with anti-DRP1 (green) or anti-TOM20 (red) antibodies. DAPI (blue) was used as a nuclear counterstaining. Middle panels show a magnification of the pictures displayed in the upper panels. Bottom images are color map representations of the pictures in the middle panels to display co-localized pixels between both fluorophores according to the color bar shown on the upper-right corner of the pictures. Warm colors depict pixels with highly correlated intensity and spatial overlap while cold colors are indicative of random or anti-correlation. Graph on the right shows the quantification of the Pearson's correlation coefficient (PCC) to display the degree of co-localization between DRP1 and TOM20 in cells transduced with the indicated factors. Red dashed line indicates the levels of DRP1 and TOM20 co-localization found in ESCs.

(D) Lysates of MEFs control or expressing OSKM, OSK, or c-MYC for 4 days were analyzed by immunoblotting using the indicated antibodies. Graphs on the right show the quantification of the data.

Data represent mean ± SEM, one-tailed unpaired t test (n = 3): *p < 0.05; **p < 0.01; ***p < 0.001; ****p < 0.0001. Scale bars, 24 μm in (B) and upper panels of (C); 12 μm in middle and bottom panels of (C). See also Figure S1.
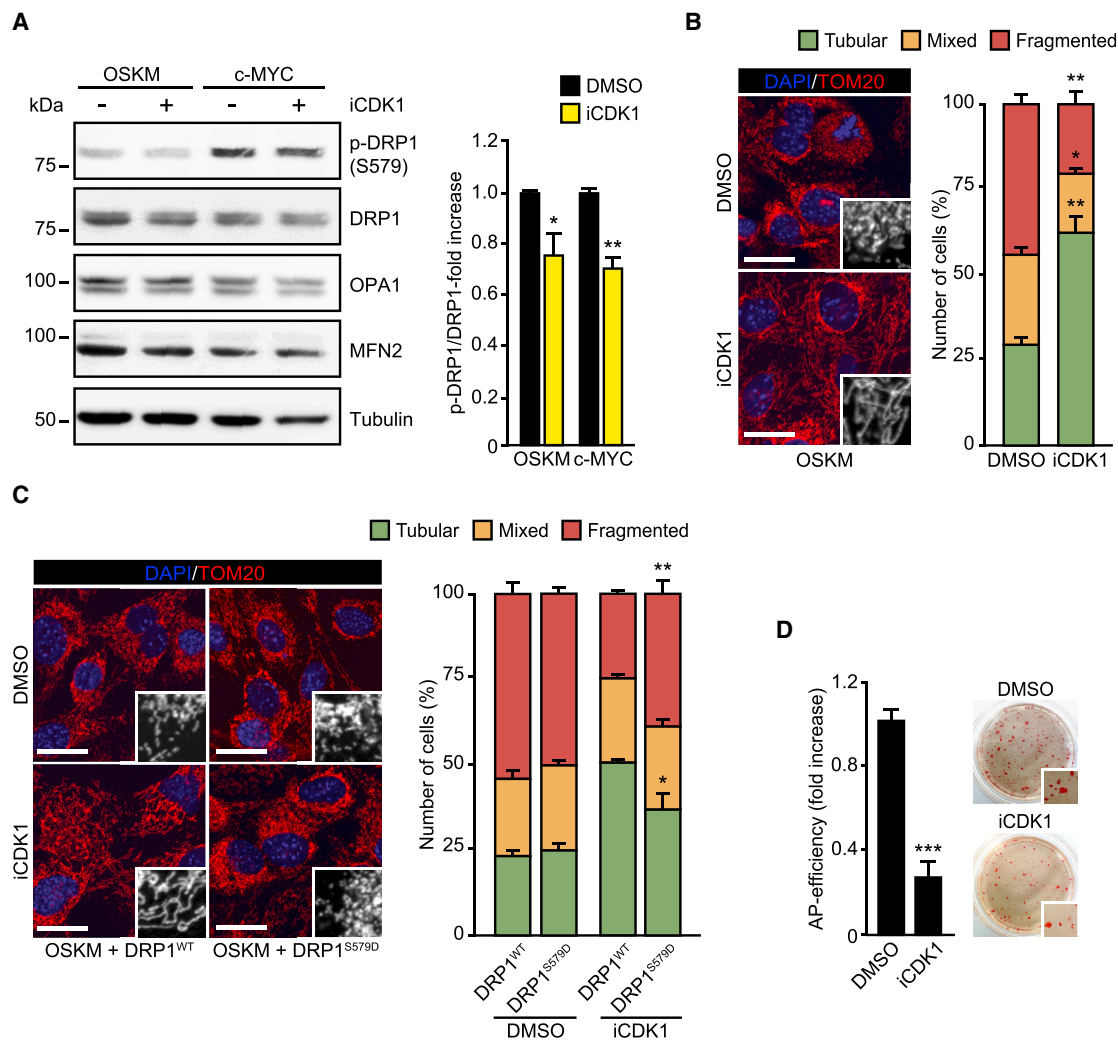
Figure 2. Role of CDK1 in c-MYC-Induced DRP1-S579 Phosphorylation

(A) Left panels: lysates from OSKM or c-MYC-transduced MEFs for 3.5 days that were incubated during 10 hr with DMSO (as vehicle control) or the CDK1 inhibitor RO-3306 (1 μM) were analyzed by immunoblotting using the indicated antibodies. Right graph shows the quantification of ERK1/2 or DRP1 phosphorylation ratios in cells treated with either DMSO (black bars) or RO-3306 (yellow bars).

(B) OSKM-transduced cells for 3.5 days were incubated with DMSO (as vehicle control) or the CDK1 inhibitor RO-3306 (1 μM) for 10 hr (iCDK1). Cells were then fixed and mitochondrial morphology assessed by immunofluorescence. Left panels: representative confocal images of MEFs stained with anti-TOM20 antibodies (red). Inset shows a black-and-white magnification of the pictures. DAPI (blue) was used as a nuclear counterstaining. Graph on the right shows the quantification of the different mitochondrial morphologies observed.

(C) Left panels show representative confocal images of MEFs expressing OSKM, together with DRP1 wild-type (DRP1^{WT}) or the phospho-mimetic S579D mutation (DRP1^{S579D}), during 3.5 days. Cells were then treated, fixed, and stained as in (B). Graph on the right shows the quantification of the indicated mitochondrial morphologies observed in the cells transduced and treated as indicated.

(D) Graphs showing the number of AP-positive colonies scored in MEFs after 25 days of OSKM retroviral delivery in the presence of DMSO (as vehicle control) or the CDK1 inhibitor RO-3306 (1 μM) (iCDK1) (panels on the right). Right panels: representative bright-field images from the plates of the indicated cultures after AP staining. Inset shows a magnification of a selected area from the AP-stained plates.

Data represent mean ± SEM, one-tailed unpaired t test (n = 3): *$p < 0.05$; **$p < 0.01$; ***$p < 0.001$. Scale bars, 24 μm in (B) and (C). See also Figure S2.

DRP1 and induces mitochondrial fission during cell division (Taguchi et al., 2007). In this regard, CDK1 inhibition (iCDK1) decreased DRP1-S579 phosphorylation in OSKM- or c-MYC-transduced cells (Figures 2A and 2B) and impaired OSKM- or c-MYC-induced mitochondrial fission (Figures 2B and S2D, respectively). Interestingly, the
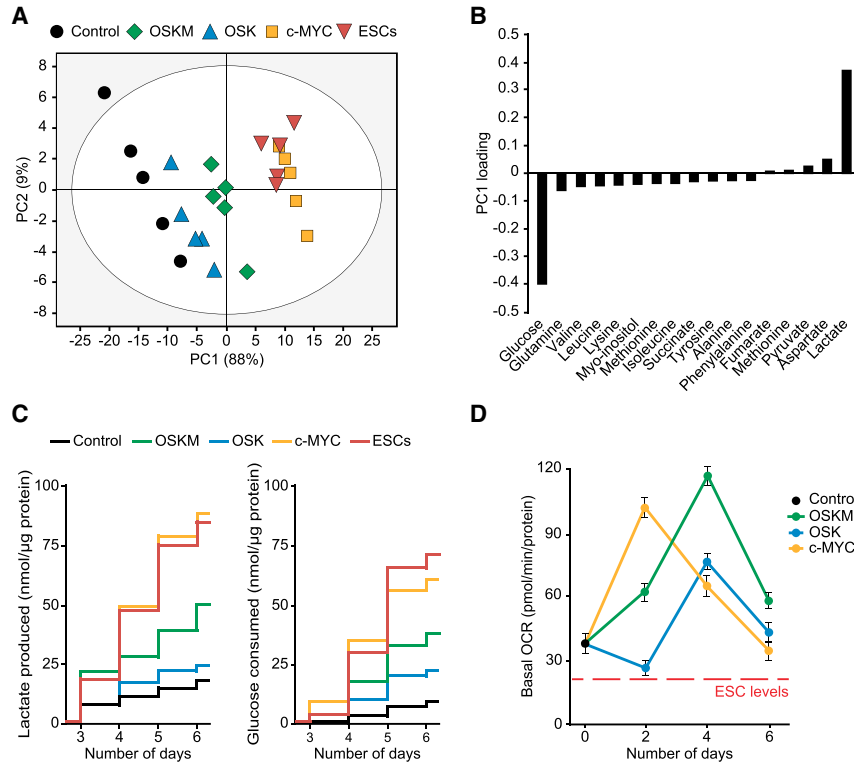
Figure 3. Glycolysis and OXPHOS Are Induced by c-MYC Early in Cell Reprogramming

(A) Principal Component 1 and 2 (PC1, PC2) projections of extracellular metabolite variations in conditioned medium taken from cells at day 4 post transduction with the indicated factors. PC1: $R^2 = 0.88$, $Q^2 = 0.84$; PC2: $R^2 = 0.08$, $Q^2 = 0.07$.

(B) Graph displaying the loadings of metabolite variations along PC1 axis.

(C) Time-course assessment of lactate accumulation (right graph) or glucose dissipation (left graph) in culture medium from ESCs or MEFs transduced with the indicated factors.

(D) Graph displaying the basal oxygen consumption rate (OCR) in MEF control or expressing the indicated factors for the days shown. Red dashed line indicates basal OCR values in ESCs.

Data represent mean ± SEM, one-tailed unpaired t test (n = 5 in A–C; n = 3 in D); all results were statistically significant (p < 0.05). See also Figures S3 and S4.

inhibition of mitochondrial fission by the CDK1 inhibitor in OSKM or c-MYC-expressing cells could be rescued by co-expression of DRP1-S579D phosphomimetic mutation but not by the wild-type form of the dynamin (Figures 2D and S2E). Furthermore, inhibition of CDK1 impaired OSKM-mediated cell reprogramming (Figure 2D). Our results therefore suggest that CDK1 collaborate with ERK1/2 in the activation of DRP1 during early cell reprogramming to induce mitochondrial fragmentation in a c-MYC-dependent manner.

A Hybrid Energetics Program Is Induced by c-MYC during Cell Reprogramming

Somatic cell metabolism is switched from oxidative- to glycolytic-based energetics during the reprogramming process (Folmes et al., 2011). We next investigated whether this metabolic change could be driven by c-MYC. For this, we first carried out a metabolomics study, based on nuclear magnetic resonance (NMR), to analyze extracellular metabolite variations in either control or OSKM-, OSK-, or c-MYC-expressing MEFs at day 4 post transduction, or in mouse embryonic stem cells (ESCs) as the endpoint control of the reprogramming process (Figures 3 and S3). Interestingly, principal component analysis (PCA) of the data showed the clustering of c-MYC-expressing MEFs with ESCs (Figure 3A). Plotting of the extracellular metabolite changes along PC1 variable revealed a deep increase in

glucose depletion and a robust accumulation of lactate in ES- and c-MYC-expressing cells (Figure 3B). Time-series measurements of lactate and glucose showed a high parallelism between c-MYC-transduced MEFs and ESCs (Figure 3C). The variation of these metabolites over time in control and OSK-transduced cells was similar, and OSKM-expressing cells showed intermediate dynamics between that of ESCs and control cells (Figure 3C). Similar trends, and c-MYC dependency, were observed when measuring the kinetics of lactate production, glucose consumption, acetate production, or glutamine consumption at day 4 of the process (Figure S3B).

These findings suggest that expression of c-MYC, alone or in combination with OSK, activates the glycolytic pathway. In fact, glycolytic flux and capacity were upregulated during the first days of OSKM expression (Figure S4A) in a c-MYC-dependent manner (Figure S4B). Our results therefore suggest that c-MYC articulates the metabolic switch associated with cell reprogramming, which has been shown to be characterized by both upregulation of glycolysis and inhibition of OXPHOS (Folmes et al., 2011).
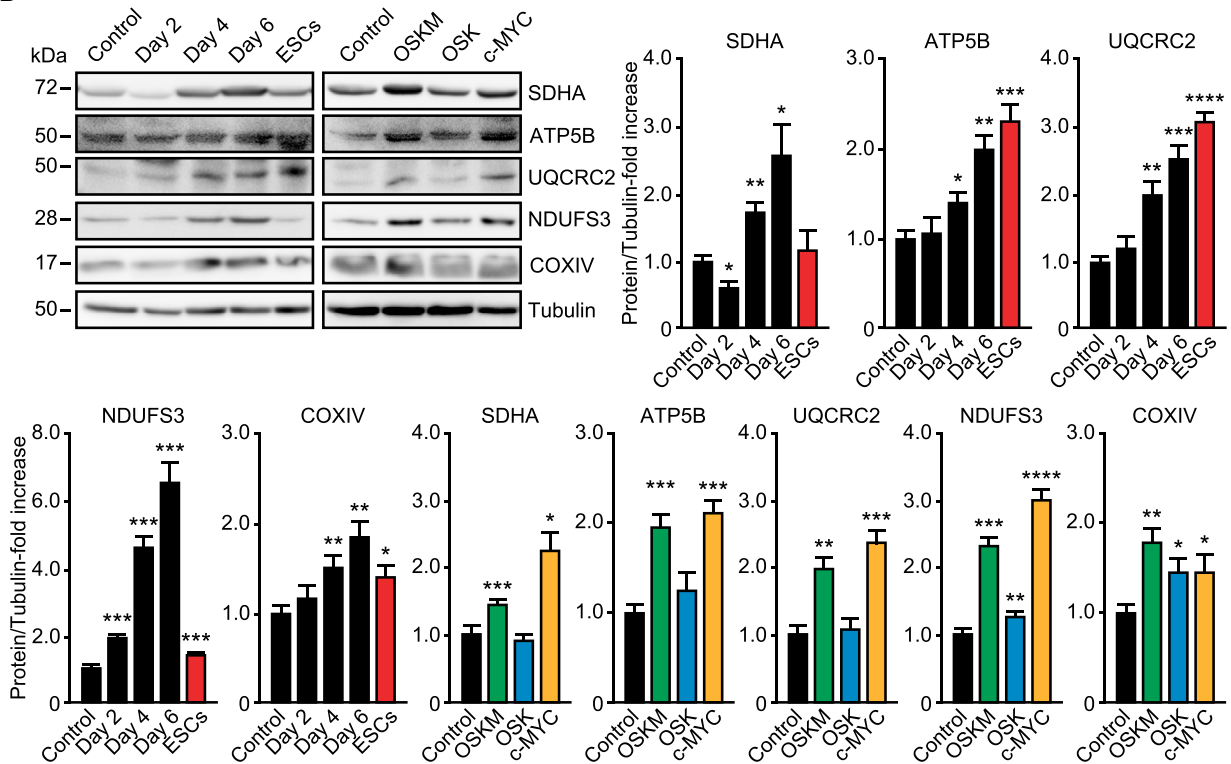
Time-course measurements of oxygen consumption rates (OCRs) revealed the induction of a transient OXPHOS peak following expression of OSKM, OSK, or c-MYC, albeit at different times and with distinctive intensities (Figure 3D). As previously reported (Kida et al., 2015), OSKM induced a robust OXPHOS peak at day 4 of reprogramming
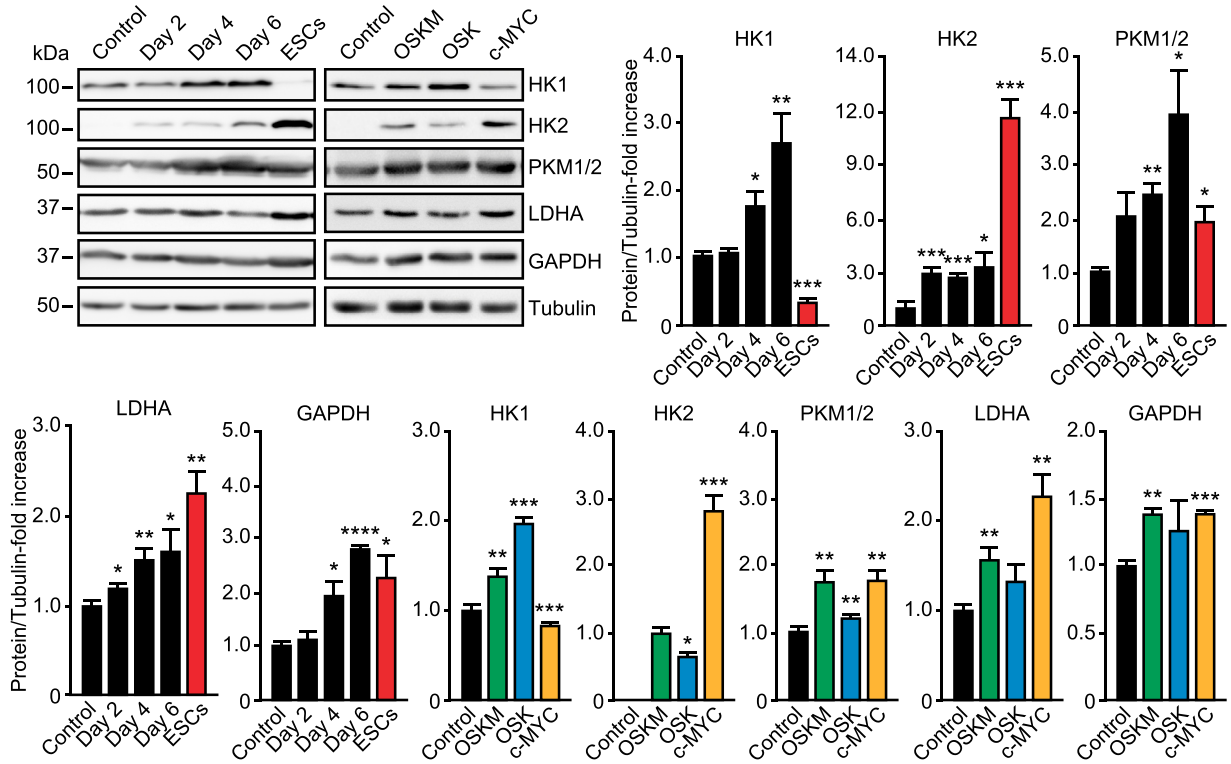
(legend on next page)

(Figures 3D and S4C). Interestingly, OSK expression also produced an OXPHOS peak at day 4, although to a much lesser extent than OSKM. Overexpression of c-MYC alone also led to an OXPHOS peak at day 2 post transduction, which was similar in intensity to that of OSKM (Figure 3D). Surprisingly, our respirometry experiments also showed that OCRs decreased at day 6 to values found at day zero, but these were not yet diminished to levels displayed by ESCs (Figure 3D). Thus, and in agreement to previously published data, our results showed that cell reprogramming induces a steady upregulation of glycolysis. However, and conversely to what was previously thought, cell reprogramming does not involve an inhibition of OXPHOS below somatic levels following the early metabolic burst. In agreement with these findings, combined immunoblotting analyses (Figure 4) and quantitative protein microarrays (Figure S5) showed that both OXPHOS and glycolysis enzymatic machineries were upregulated during early cell reprogramming in a c-MYC-dependent manner.

Mitochondrial Membrane Potential Marks Cells Prone to Cell Reprogramming

We next sought to investigate the importance of maintaining somatic OXPHOS rates for cell reprogramming. First, we wanted to assess mitochondrial membrane potential (MMP), as an indicator of mitochondrial function, using the TMRM probe. Flow-cytometry analyses revealed elevated MMP levels in pluripotent cells compared with controls (Figure 5A). Immunofluorescence examination of MMP also showed that ESCs displayed high TMRM levels compared with controls (Figure 5B). As previously reported (Folmes et al., 2011), we observed colonies with intense TMRM staining in OSKM-expressing cells at day 12 post transduction (Figure 5B). These TMRM-positive colonies were also positive for SSEA-1 staining, suggesting that functional mitochondria are important for cells undergoing reprogramming. As we have recently described (Prieto et al., 2016a), total mitochondrial content, measured by flow cytometry using the MMP-independent probe MitoTracker green, was reduced in pluripotent cells compared with control cells (Figure S6A) and decreased with time in either OSKM-, OSK-, or c-MYC-transduced cells (Figures S6B and S6C). These observations led us to take into consideration this feature when analyzing MMP by this technique (see below). Time-course examination of TMRM/MitoTracker green ratios in OSK- or OSKM-expressing cells showed a gradual increase in the relative MMP that reached a plateau

at day 6, OSKM inducing a higher increase in these ratios than OSK (Figure 5C). Interestingly, the relative MMP values observed in OSKM-expressing cells were higher than those found in either somatic or OSK-expressing cells. Relative MMP in cells expressing c-MYC alone displayed a steep increase, which peaked at day 4 and decreased at day 6 (Figure 5C). Interestingly, we observed an upregulation of the ATPase inhibitor factor 1 (ATPIF1), a physiological inhibitor of the H^+-ATP synthase (Gledhill et al., 2007), during OSKM-induced cell reprogramming (Figure 5D, upper panels). Expression of ATPIF1 protein was reduced by OSK and highly increased by either OSKM or c-MYC (Figure 5D, lower panels). Furthermore, knockdown of ATPIF1 protein (Figure S6D) reduced the emergence of AP-positive colonies in OSKM-transduced cells by ~30% (Figure 5E). Taken together, these results suggest that elevated MMP, induced by c-MYC and likely upheld by ATPIF1-mediated inhibition of the ATPase, could mark cells prone to cell reprogramming.

To investigate this possibility, we sorted OSKM-expressing cells based on their TMRM intensity at either day 6 or day 12 post transduction (Figure 6A) and compared their ability to generate AP-positive colonies as an estimation of reprogramming efficiency. OSKM-expressing TMRM-high cell population sorted at day 6 post transduction showed ~25% increase in the number of AP-positive colonies when compared with TMRM-low counterparts (Figure 6B). Remarkably, this increase in the reprogramming efficiency shown by TMRM-high cells was clearly evident when OSKM-expressing cells were sorted at day 12 post transduction, and TRMR-high cells displayed a >10-fold increase in the number of AP-positive colonies (Figure 6C). These results suggest that high MMP marks cells prone to reprogramming.

We next examined the metabolic profiles of these OSKM-expressing cell populations displaying different MMPs. Cell sorting was performed at day 6 (Figures 6D and S6E) or day 12 (Figures 6E and S6F) post transduction into TMRM-low (blue bars and lines) and TMRM-high (red bars and lines) cell populations. TMRM-low cells sorted at either day 6 or day 12 post transduction displayed similar (day 6) or reduced (day 12) OCRs and glycolytic rates compared with controls. Remarkably, TMRM-high cell populations sorted at either day 6 or day 12 post transduction showed increased OCRs and glycolytic rates. Furthermore, transient inhibition of ETC complex I by rotenone at different days of the process blunted cell reprogramming

Figure 4. Induction of Glycolytic and OXPHOS Enzymes by c-MYC
(A and B) Lysates of ESCs, MEFs control, or expressing OSKM for the specified days (left panels, black and red bars), or the indicated factors for 4 days (right panels, colored bars), were analyzed by immunoblotting using antibodies against the glycolytic (A) or OXPHOS (B) enzymes shown. Graphs show the quantification of the data. Data represent mean ± SEM, one-tailed unpaired t test (n = 3): *p < 0.05; **p < 0.01; ***p < 0.001; ****p < 0.0001. See also Figure S5.
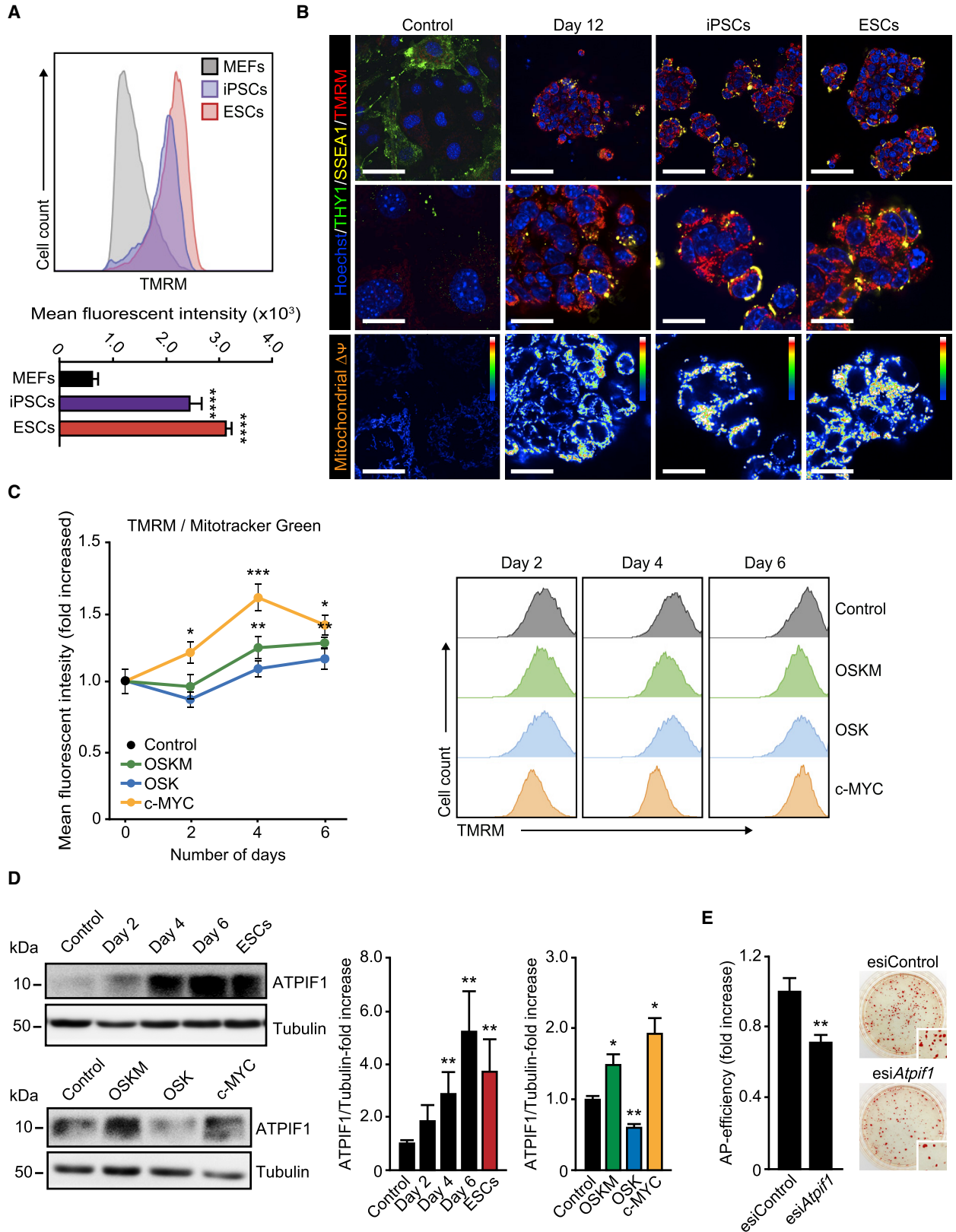
(legend on next page)

(Figure 6F), underscoring the importance of OXPHOS for cell reprogramming. Taken together, our results indicate that both glycolysis and OXPHOS play central roles in the phenotypic transition of somatic cells to pluripotency.

DISCUSSION

It has been reported that overexpression of exogenous c-MYC is beneficial but not necessary for cell reprogramming (Nakagawa et al., 2008; Wernig et al., 2008). Moreover, it has been shown that MYC family members do not directly regulate pluripotency in ESCs or mouse embryos (Scognamiglio et al., 2016). These findings have nourished the idea that MYC does not play a major role in cell reprogramming. Here we present evidence showing that MYC is necessary for cell reprogramming, likely by inducing a hybrid energetics program to favor the phenotypic transition to pluripotency.

Somatic cells undergo a dramatic remodeling in their metabolic profiles during their transit to pluripotency (Folmes et al., 2011). It has been suggested that this metabolic transition is a synchronous phenomenon in which a gradual increase in glycolytic flux parallels a reduction in cellular respiration during the reprogramming process (Folmes et al., 2011; Panopoulos et al., 2012; Varum et al., 2011). However, we found that a hybrid OXPHOS/glycolysis metabolic phenotype, similar to that found in naive pluripotent stem cells (Takashima et al., 2014; Zhou et al., 2012), is generated early during the process by c-MYC and marks cells prone to cell reprogramming.

The upregulation of both glycolytic and OXPHOS enzymes by c-MYC (Sridharan et al., 2009; Hansson et al., 2012; Cao et al., 2015; Sone et al., 2017; and this study) may account for the elevated OXPHOS and glycolytic activities observed during early cell reprogramming. OSKM expression causes an early and transient activation peak of OXPHOS (Kida et al., 2015; Sone et al., 2017; and this study), which we found is induced by the combined activity of OSK and c-MYC. The steep OXPHOS downregulation to near somatic levels observed in these studies coincided with the upregulation of glycolytic fluxes. The opposite dynamics in the activity of these two pathways could suggest the negative regulation of OXPHOS by high glycolytic metabolic rates, which may limit pyruvate availability in mitochondria to maximize NAD^+ recycling. However, an orchestrated regulation of both pathways by the crosstalk of different gene expression programs induced by the reprogramming factors could not be ruled out. In this regard, the upregulation of ATPIF1 protein by c-MYC may play a role in modulating OXPHOS activity, as it does in cancer cells (Santacatterina et al., 2016). Although necessary for cell reprogramming (Kida et al., 2015 and this study), whether this OXPHOS peak is solely a by-product of the forced expression of the reprogramming factors or plays a specific role in the process remains unknown. In this regard, it is possible that the surge in OXPHOS could induce a burst in reactive oxygen species (ROS) during cell reprogramming (Esteban et al., 2010). As ROS can activate pro-proliferative signaling pathways (Hawkins et al., 2016; Reczek and Chandel, 2015), an early and transitory increase in ROS levels could stimulate cell proliferation and therefore be favorable for cell reprogramming. In keeping with this, optimal ROS signaling has been found to be critical for nuclear reprogramming (Zhou et al., 2016). Remarkably, our observations showing that cells displaying high MMP are prone to cell reprogramming underscore the role of mitochondria in this process. These high MMP cells displayed both increased glycolysis and somatic OXPHOS rates, which indicates that a hybrid metabolism is readily

Figure 5. Increased Mitochondria Polarization during Cell Reprogramming
(A) Representative flow-cytometry histograms of MEFs, induced pluripotent stem cells (iPSCs), and ESCs stained with TMRM to assess mitochondrial membrane potential. Graph underneath shows the quantification of the mean fluorescence intensity of the histograms shown above.
(B) Representative confocal images of live MEFs before (Control) or 12 days after OSKM expression (Day 12), iPSCs, and ESCs stained with anti-THY1 (green) or anti-SSEA1 (yellow) antibodies, combined with the cell-permeable TMRM dye (red). Hoechst 33342 (blue) was used as a nuclear counterstaining. Lower pictures are color map representations of the pictures in the middle panels showing TMRM intensity according to the displayed color bar. Scale bars, 24 μm (upper images) and 12 μm (middle and bottom images).
(C) Right: histograms of TMRM staining in MEFs expressing the indicated factors for the days shown. Left graph represents the TMRM/MitoTracker green ratio dynamics along the indicated days.
(D) Lysates of MEF control, expressing OSKM for the specified days or ESCs (upper panels, black and red bars in the right graph), or the indicated factors for 4 days (lower panels, colored bars in the right graph) were analyzed by immunoblotting using the shown antibodies. Graphs on the right show the quantification of the data.
(E) MEFs transduced with OSKM factors were transfected with esiRNAs targeting either *eGFP* (Control) or *Atpif1* at day 1 post transduction. Graph shows the number of AP-positive colonies obtained after 25 days of retroviral delivery. Panels on the right show representative bright-field images from the plates of the indicated cultures after AP staining; inset shows magnification of a selected area from the AP-stained plates.
Data represent mean ± SEM, one-tailed unpaired t test (n = 3): *p < 0.05; **p < 0.01; ***p < 0.001; ****p < 0.0001. See also Figure S6.
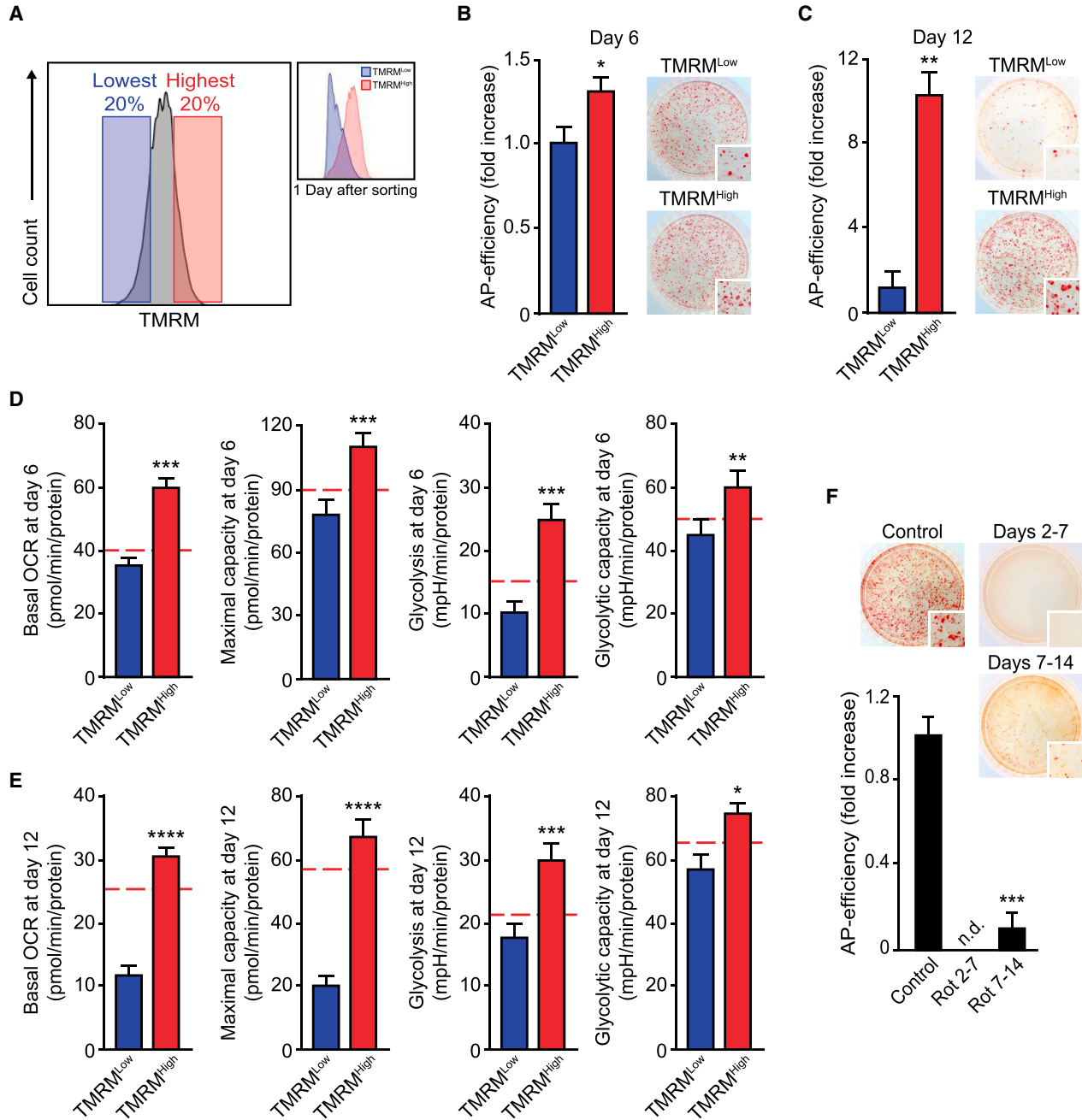
Figure 6. Cells Prone to Reprogramming Display a Hybrid Metabolism

(A) Flow-cytometry histograms illustrating the windows used for sorting OSKM-expressing cells based on their TMRM staining intensity (left histograms) and the TMRM profiles following overnight culture of the sorted cells at the indicated days post transduction (right histograms).

(B and C) Graphs showing the number of AP-positive colonies scored in MEFs after 25 days of OSKM retroviral delivery that were sorted based on their TMRM loading intensity (TMRM^{Low} or TMRM^{High}) at day 6 (B) or day 12 (C) post transduction. Right panels: representative bright-field images from the plates of the indicated cultures after AP staining. Inset shows magnification of a selected area from the AP-stained plates.

(D and E) Graphs displaying basal oxygen rate (OCR), maximal respiratory capacity, glycolytic flux (Glycolysis), or the glycolytic capacity of OSKM-transduced cells sorted as above at day 6 (D) or day 12 (E) post transduction. Dashed red lines show the values of the mean, corresponding to non-transduced MEF controls in each assay.

(legend continued on next page)

established during the first stages of cell reprogramming, likely by c-MYC.

Overall, our work showing the early events driving the metabolic rewiring by MYC reinforce the existent parallels between cell reprogramming and tumorigenesis (Abad et al., 2013; Apostolou and Hochedlinger, 2013; Hochedlinger et al., 2005; Mosteiro et al., 2016; Ohnishi et al., 2014; Prieto and Torres, 2017). Also, our findings suggest that variation of endogenous MYC levels is a determining factor for cell reprogramming mediated by either forced OSK expression or chemical cocktails, in line with studies in other biological contexts (Clavería et al., 2013; Sancho et al., 2013).

EXPERIMENTAL PROCEDURES

Cell Culture, Reprogramming Assays, Reagents, and Plasmids

The induced pluripotent stem cell lines used in this study have been described elsewhere (Prieto et al., 2016a, 2016b) and were grown in gelatinized plates in high-glucose DMEM supplemented with 10% fetal bovine serum (FBS), 1× non-essential amino acids, 1× sodium pyruvate, 1× penicillin/streptomycin (all from Biowest), 0.1 mM 2-mercaptoethanol (Sigma), in the presence of human leukemia inhibitory factor (prepared in-house). Wild-type MEFs (homogeneous C57BL/6 background) were prepared from E13.5 pooled embryos and cultured in high-glucose DMEM supplemented with 10% FBS and 1× penicillin/streptomycin. Early-passage MEFs (third passage at most) were used in all experiments. All procedures were carried out in accordance with the guidelines of the Ethics committee at the University of Valencia. Mice were crossed and maintained at the University of Valencia animal core facility in accordance with Spanish regulations (RD53/2013). The experimental protocol (no. 2015/VSC/PEA/00,079) was approved by the Animal Experimentation Ethics Committee of the University of Valencia and the Generalitat Valenciana government (Spain). Retroviral constructs pMX-*Oct4*, pMX-*Sox2*, pMX-*Klf4*, and pMX-*c-Myc* (Takahashi and Yamanaka, 2006) were from Addgene. All cells have been routinely tested for mycoplasma contamination using the Lookout MYCoplasma PCR detection kit (Sigma-Aldrich).

Reprogramming was carried out by transduction of MEFs with retroviruses encoding OCT4, SOX2, KLF4, and c-MYC as previously described (Prieto et al., 2016a, 2016b; Takahashi and Yamanaka, 2006). Reprogramming was assessed 25 days after transduction of MEFs with OSKM or OSK-encoding retroviruses by scoring all the AP-positive colonies per 60 mm. AP staining was performed according to the manufacturer's instructions (Alkaline Phosphatase Detection Kit, Millipore). See Supplemental Experimental Procedures.

Immunofluorescence and Flow Cytometry

For live immunofluorescence analysis, cells were plated on gelatin-coated tissue culture dishes. Cells, untreated or transduced with the indicated viruses, were plated at 1.5×10^4 cells/cm^2 the day before processing. The cells were incubated with the indicated antibodies diluted in fresh culture medium for 45 min at 37°C in a CO_2 incubator. Cells were then washed three times and medium replaced with fresh culture medium containing 100 nM TMRM (tetramethylrhodamine methyl ester) and 2 μg/mL of cell-permeable Hoechst 33,342 (both from Thermo Fisher) for 30 min in a CO_2 incubator at 37°C. Cells were washed three times with fresh medium and analyzed immediately by confocal microscopy.

Confocal immunofluorescence images were taken using a Fluoview FV10i confocal microscope equipped with 405-, 488-, and 633-nm lasers and a live cell environmental module (Olympus). Three-dimensional reconstructions of z stacks and color map representations of the images were performed using FV10-ASW 2.1 viewer software. Co-localization of TOM20 and DRP1 staining was evaluated by calculating the Pearson's correlation coefficient using the freely available JACoP plug-in (http://rsb.info.nih.gov/ij/plugins/track/jacop.html) for ImageJ analysis software. All images were compiled using Adobe Illustrator CS5.

For assessing or sorting cells based on their MMP by flow cytometry, cells treated as indicated in the text were trypsinized, resuspended in culture medium containing 1% FBS and 100 nM TMRR, and incubated at 37°C in an incubator with CO_2 supply for 15 min. Cells were then processed for analysis or cell sorting by flow cytometry. Analytical flow-cytometry measurements were taken using a FACSVerse flow cytometer (BD Biosciences) and analyzed using FlowJo software (Tree Star). At least 10,000 events from each sample were recorded. Fluorescence-activated cell sorting based on TMRM intensity was carried out using a FACSAria III (Becton Dickinson). Details about the antibodies used in this study are provided in Tables S1 and S2.

Western Blot

Cells transduced as indicated in the main text were lysed in RIPA buffer (50 mM Tris [pH 7.5], 150 mM NaCl, 0.1% SDS, 1% Triton X-100, 0.5% sodium deoxycholate, 100 mM NaF, 2 mM Na$_3$VO$_4$, 20 mM Na$_4$P$_2$O$_7$, and 1× complete proteinase inhibitor cocktail from Roche). Cellular lysates were used for immunoblotting with the indicated antibodies using standard procedures (see Supplemental Experimental Procedures). Details about the antibodies used in this study are provided in Tables S1 and S2.

Printing and Processing of Reverse-Phase Protein Arrays

The protein concentration of the samples was determined with the Bradford reagent (Bio-Rad) using BSA as standard, and diluted in PBS (137 mM NaCl, 2.7 mM KCl, 10 mM Na$_2$HPO$_4$ and 1.8 mM

(F) Graph showing the scoring of AP-positive colonies obtained in MEFs after 25 days of OSKM retroviral delivery incubated with DMSO (as vehicle control), or the ETC complex I inhibitor rotenone (0.5 μM) for the indicated days. Right panels: representative bright-field images from the plates of the indicated cultures after AP staining; inset shows magnification of a selected area from the AP-stained plates. Data represent mean ± SEM, one-tailed unpaired t test (n = 3): *p < 0.05; **p < 0.01; ***p < 0.001; ****p < 0.0001; n.d., not detected. See also Figure S6.

KH$_2$PO$_4$ [pH 7.4]) to a final protein concentration of 0.5 μg/μL before printing. After printing, arrays were allowed to dry and further blocked in PBS with Tween 20 containing 5% skimmed milk. Thereafter, each pad in the array was incubated overnight at 4°C with the indicated concentrations of highly specific primary monoclonal or polyclonal antibodies. Microarrays were scanned using a Typhoon 9410 scanner (GE Healthcare). Details of the antibodies used can be found in Tables S1 and S2.

Nucleic Acid Purification and qPCR Analysis

Total RNA was extracted using TRIzol reagent and cDNA synthesized using a SuperScript III reverse transcriptase kit (both from Invitrogen). cDNA products were amplified using an Applied Biosystems StepOne plus Fast Real-Time PCR System. Sequences of the oligonucleotides used in this study are listed in Table S3 and correspond to predesigned KiCqStart SYBR Green primers (Sigma-Aldrich).

Metabolomic Footprinting

Metabolic profiling of cellular medium was carried out with NMR spectroscopy. Samples of culture medium were collected 10, 24, 48, and 72 hr after initial cell incubation with fresh medium at day 2.5 post transduction. Metabolite assignment was performed with the help of the Human Metabolome database and published literature. Metabolite concentrations in basal media were subtracted from concentrations of metabolites in 10- to 72-hr conditioned media for the calculation of net fluxes. The resulting rates were normalized to total cellular protein content determined by a BCA protein assay (Pierce, Thermo-Scientific). See Supplemental Experimental Procedures for details.

Extracellular Metabolic Flux Analysis

Basal and uncoupled OCR, or extracellular acidification rate (ECAR), were measured using a Seahorse bioanalyzer (XF96) and the Mito or Glycolysis stress test kits (both from Seahorse Bioscience, Millipore), respectively, using 20,000–30,000 cells per well. Each experiment was conducted in triplicate, repeated at least three times, and normalized to total protein contents. See Supplemental Experimental Procedures for details.

Statistical Methods

Principal component analysis was performed on Pareto scaled and mean centered data using SIMCA-p+ 12.0 PCA (Umetrics). The model quality was assessed by R2 (goodness of fit) and Q2 (goodness of prediction).

Where indicated, Student's t test was used to estimate statistical significance between categories. Relative values (percentages) were normalized using arcsine transformation before carrying out their statistical comparison. Results are presented as mean ± SEM or mean ± SD as indicated. The number of independent experiments used to estimate statistical significance is denoted as "n" in every figure legend.

SUPPLEMENTAL INFORMATION

Supplemental Information includes Supplemental Experimental Procedures, six figures, and three tables and can be found with this article online at https://doi.org/10.1016/j.stemcr.2018.10.018.

REFERENCES

Abad, M., Mosteiro, L., Pantoja, C., Cañamero, M., Rayon, T., Ors, I., Graña, O., Megías, D., Domínguez, O., Martínez, D., et al. (2013). Reprogramming in vivo produces teratomas and iPS cells with totipotency features. Nature *502*, 340–345.

Apostolou, E., and Hochedlinger, K. (2013). Chromatin dynamics during cellular reprogramming. Nature *502*, 462–471.

Bretones, G., Delgado, M.D., and León, J. (2015). MYC and cell cycle control. Biochim. Biophys. Acta *1849*, 506–516.

Buganim, Y., Faddah, D.A., Cheng, A.W., Itskovich, E., Markoulaki, S., Ganz, K., et al. (2012). Single-cell expression analyses during cellular reprogramming reveal an early stochastic and a late hierarchic phase. Cell *150*, 1209–1222.

Cao, Y., Guo, W.T., Tian, S., He, X., Wang, X.W., Liu, X., Gu, K.L., Ma, X., Huang, D., Hu, L., et al. (2015). miR-290/371-Mbd2-MYC circuit regulates glycolytic metabolism to promote pluripotency. EMBO J. *34*, 609–623.

Clavería, C., Giovinazzo, G., Sierra, R., and Torres, M. (2013). MYC-driven endogenous cell competition in the early mammalian embryo. Nature *500*, 39–44.

Dang, C.V. (2016). A time for MYC: metabolism and therapy. Cold Spring Harb. Symp. Quant. Biol. *81*, 79–83.

Esteban, M.A., Wang, T., Qin, B., Yang, J., Qin, D., Cai, J., Li, W., Weng, Z., Chen, J., Ni, S., et al. (2010). Vitamin C enhances the generation of mouse and human induced pluripotent stem cells. Cell Stem Cell *6*, 71–79.

Folmes, C.D., Nelson, T.J., Martinez-Fernandez, A., Arrell, D.K., Lindor, J.Z., Dzeja, P.P., Ikeda, Y., Perez-Terzic, C., and Terzic, A. (2011). Somatic oxidative bioenergetics transitions into pluripotency-dependent glycolysis to facilitate nuclear reprogramming. Cell Metab. 14, 264–271.

Gledhill, J.R., Montgomery, M.G., Leslie, A.G., and Walker, J.E. (2007). How the regulatory protein, IF(1), inhibits F(1)-ATPase from bovine mitochondria. Proc. Natl. Acad. Sci. U S A 104, 15671–15676.

Hansson, J., Rafiee, M.R., Reiland, S., Polo, J.M., Gehring, J., Okawa, S., Huber, W., Hochedlinger, K., and Krijgsveld, J. (2012). Highly coordinated proteome dynamics during reprogramming of somatic cells to pluripotency. Cell Rep. 2, 1579–1592.

Hawkins, K.E., Joy, S., Delhove, J.M., Kotiadis, V.N., Fernandez, E., Fitzpatrick, L.M., Whiteford, J.R., King, P.J., Bolanos, J.P., Duchen, M.R., et al. (2016). NRF2 orchestrates the metabolic shift during induced pluripotent stem cell reprogramming. Cell Rep. 14, 1883–1891.

Hochedlinger, K., Yamada, Y., Beard, C., and Jaenisch, R. (2005). Ectopic expression of Oct-4 blocks progenitor-cell differentiation and causes dysplasia in epithelial tissues. Cell 121, 465–477.

Kida, Y.S., Kawamura, T., Wei, Z., Sogo, T., Jacinto, S., Shigeno, A., Kushige, H., Yoshihara, E., Liddle, C., Ecker, J.R., et al. (2015). ERRs mediate a metabolic switch required for somatic cell reprogramming to pluripotency. Cell Stem Cell 16, 547–555.

Kidger, A.M., and Keyse, S.M. (2016). The regulation of oncogenic Ras/ERK signalling by dual-specificity mitogen activated protein kinase phosphatases (MKPs). Semin. Cell Dev. Biol. 50, 125–132.

Kress, T.R., Sabò, A., and Amati, B. (2015). MYC: connecting selective transcriptional control to global RNA production. Nat. Rev. Cancer 15, 593–607.

Mosteiro, L., Pantoja, C., Alcazar, N., Marión, R.M., Chondronasiou, D., Rovira, M., Fernandez-Marcos, P.J., Muñoz-Martin, M., Blanco-Aparicio, C., Pastor, J., et al. (2016). Tissue damage and senescence provide critical signals for cellular reprogramming in vivo. Science 354. https://doi.org/10.1126/science.aaf4445.

Nakagawa, M., Koyanagi, M., Tanabe, K., Takahashi, K., Ichisaka, T., Aoi, T., Okita, K., Mochiduki, Y., Takizawa, N., and Yamanaka, S. (2008). Generation of induced pluripotent stem cells without MYC from mouse and human fibroblasts. Nat. Biotechnol. 26, 101–106.

Ohnishi, K., Semi, K., Yamamoto, T., Shimizu, M., Tanaka, A., Mitsunaga, K., Okita, K., Osafune, K., Arioka, Y., Maeda, T., et al. (2014). Premature termination of reprogramming in vivo leads to cancer development through altered epigenetic regulation. Cell 156, 663–677.

Panopoulos, A.D., Yanes, O., Ruiz, S., Kida, Y.S., Diep, D., Tautenhahn, R., Herrerías, A., Batchelder, E.M., Plongthongkum, N., Lutz, M., et al. (2012). The metabolome of induced pluripotent stem cells reveals metabolic changes occurring in somatic cell reprogramming. Cell Res. 22, 168–177.

Polo, J.M., Anderssen, E., Walsh, R.M., Schwarz, B.A., Nefzger, C.M., Lim, S.M., et al. (2012). A molecular roadmap of reprogramming somatic cells into iPS cells. Cell 151, 1617–1632.

Prieto, J., and Torres, J. (2017). Mitochondrial dynamics: in cell reprogramming as it is in cancer. Stem Cells Int. 2017, 8073721.

Prieto, J., León, M., Ponsoda, X., Sendra, R., Bort, R., Ferrer-Lorente, R., Raya, A., López-García, C., and Torres, J. (2016a). Early ERK1/2 activation promotes DRP1-dependent mitochondrial fission necessary for cell reprogramming. Nat. Commun. 7, 11124.

Prieto, J., León, M., Ponsoda, X., García-García, F., Bort, R., Serna, E., Barneo-Muñoz, M., Palau, F., Dopazo, J., López-García, C., et al. (2016b). Dysfunctional mitochondrial fission impairs cell reprogramming. Cell Cycle 15, 3240–3250.

Reczek, C.R., and Chandel, N.S. (2015). ROS-dependent signal transduction. Curr. Opin. Cell Biol. 33, 8–13.

Ríos, P., Nunes-Xavier, C.E., Tabernero, L., Köhn, M., and Pulido, R. (2014). Dual-specificity phosphatases as molecular targets for inhibition in human disease. Antioxid. Redox Signal. 20, 2251–2273.

Sancho, M., Di-Gregorio, A., George, N., Pozzi, S., Sánchez, J.M., Pernaute, B., and Rodríguez, T.A. (2013). Competitive interactions eliminate unfit embryonic stem cells at the onset of differentiation. Dev. Cell 26, 19–30.

Santacatterina, F.L., Sánchez-Cenizo, L., Formentini, M.A., Mobasher, E., Casas, C.B., Rueda, I., Martínez-Reyes, I., Núñez de Arenas, C., García-Bermúdez, J., Zapata, J.M., et al. (2016). Downregulation of oxidative phosphorylation in the liver by expression of the ATPase inhibitory factor 1 induces a tumor-promoter metabolic state. Oncotarget 7, 490–508.

Scognamiglio, R., Cabezas-Wallscheid, N., Thier, M.C., Altamura, S., Reyes, A., Prendergast, Á.M., Baumgärtner, D., Carnevalli, L.S., Atzberger, A., Haas, S., et al. (2016). MYC depletion induces a pluripotent dormant state mimicking diapause. Cell 164, 668–680.

Sone, M., Morone, N., Nakamura, T., Tanaka, A., Okita, K., Woltjen, K., Nakagawa, M., Heuser, J.E., Yamada, Y., Yamanaka, S., et al. (2017). Hybrid cellular metabolism coordinated by Zic3 and Esrrb synergistically enhances induction of naive pluripotency. Cell Metab. 25, 1103–1117.e6.

Sridharan, R., Tchieu, J., Mason, M.J., Yachechko, R., Kuoy, E., Horvath, S., Zhou, Q., and Plath, K. (2009). Role of the murine reprogramming factors in the induction of pluripotency. Cell 136, 364–377.

Taguchi, N., Ishihara, N., Jofuku, A., Oka, T., and Mihara, K. (2007). Mitotic phosphorylation of dynamin-related GTPase DRP1 participates in mitochondrial fission. J. Biol. Chem. 282, 11521–11529.

Takahashi, K., and Yamanaka, S. (2006). Induction of pluripotent stem cells from mouse embryonic and adult fibroblast cultures by defined factors. Cell 126, 663–676.

Takashima, Y., Guo, G., Loos, R., Nichols, J., Ficz, G., Krueger, F., Oxley, D., Santos, F., Clarke, J., Mansfield, W., et al. (2014). Resetting transcription factor control circuitry toward ground-state pluripotency in human. Cell 158, 1254–1269.

Varum, S., Rodrigues, A.S., Moura, M.B., Momcilovic, O., Easley, C.A., 4th, Ramalho-Santos, J., Van Houten, B., and Schatten, G. (2011). Energy metabolism in human pluripotent stem cells and their differentiated counterparts. PLoS One 6, e20914.

Wernig, M., Meissner, A., Cassady, J.P., and Jaenisch, R. (2008). c-MYC is dispensable for direct reprogramming of mouse fibroblasts. Cell Stem Cell *2*, 10–12.

Zhou, W., Choi, M., Margineantu, D., Margaretha, L., Hesson, J., Cavanaugh, C., Blau, C.A., Horwitz, M.S., Hockenbery, D., Ware, C., et al. (2012). HIF1α induced switch from bivalent to exclusively glycolytic metabolism during ESC-to-EpiSC/hESC transition. EMBO J. *31*, 2103–2116.

Zhou, G., Meng, S., Li, Y., Ghebre, Y.T., and Cooke, J.P. (2016). Optimal ROS signaling is critical for nuclear reprogramming. Cell Rep. *15*, 919–925.

Zhuang, Q., Li, W., Benda, C., Huang, Z., Ahmed, T., Liu, P., Guo, X., Ibañez, D.P., Luo, Z., Zhang, M., et al. (2018). NCoR/SMRT co-repressors cooperate with c-MYC to create an epigenetic barrier to somatic cell reprogramming. Nat. Cell Biol. *20*, 400–412.

Supplemental Information

MYC Induces a Hybrid Energetics Program Early in Cell Reprogramming

Javier Prieto, Arnold Y. Seo, Marian León, Fulvio Santacatterina, Laura Torresano, Martina Palomino-Schätzlein, Karen Giménez, Azahara Vallet-Sánchez, Xavier Ponsoda, Antonio Pineda-Lucena, José M. Cuezva, Jennifer Lippincott-Schwartz, and Josema Torres

SUPPLEMENTAL INFORMATION

Supplemental information accompanying this paper includes:

- ➢ 6 Supplemental Figures:

  - • S1, related to Figure 1.

  - • S2, related to Figure 2.

  - • S3 and S4, related to Figure 3.

  - • S5, related to Figure 4

  - • S6, related to Figures 5 and 6.

- ➢ Supplemental Experimental Procedures

- ➢ Supplemental References, related to Supplemental Experimental Procedures.

- ➢ 3 Supplemental Tables:

  - • Table S1, primary antibodies used in this study.

  - • Table S2, secondary antibodies used in this study.

  - • Table S3, sequence of the primers used in this study.
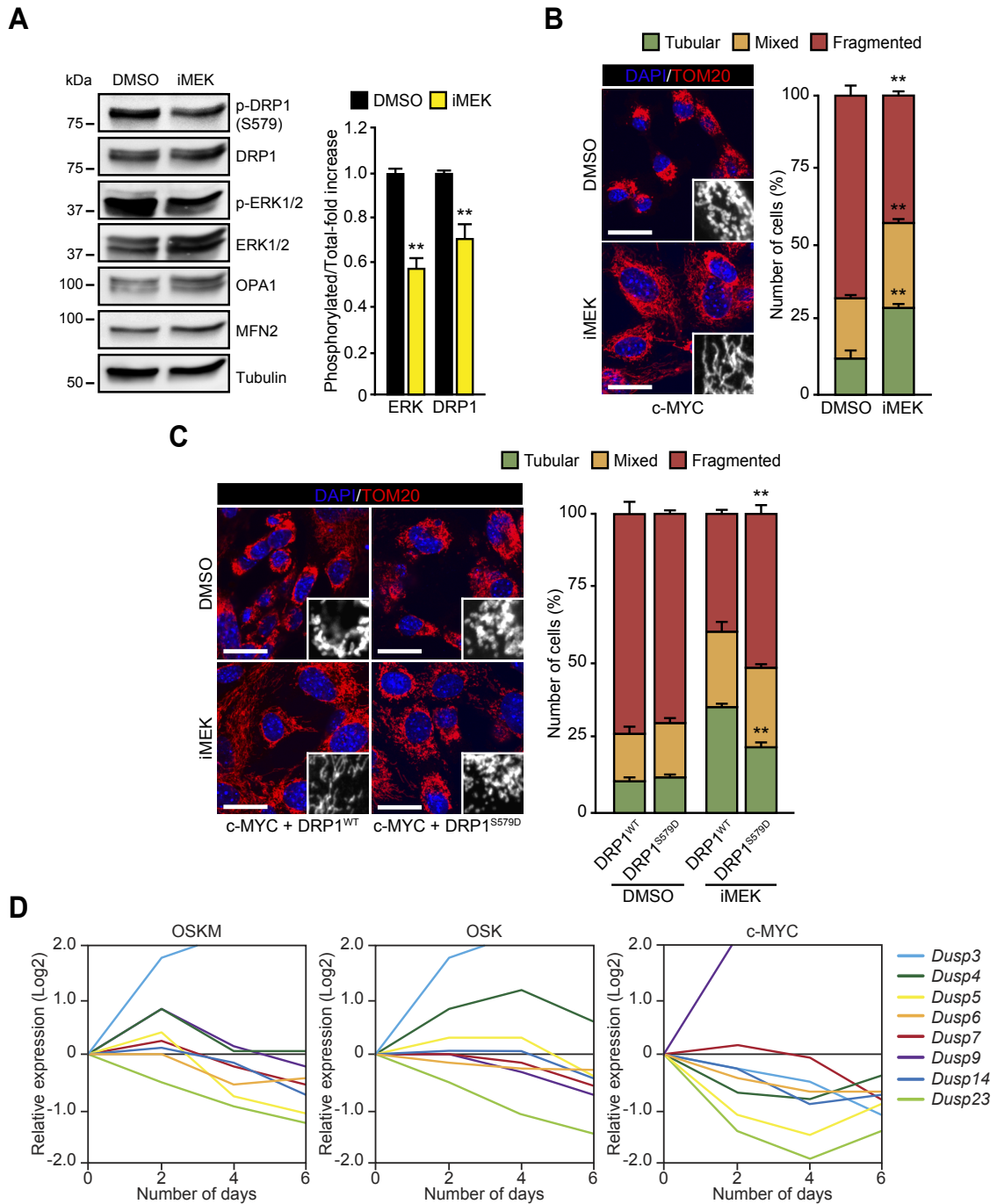
Figure S1. Role of c-MYC in ERK1/2-induced mitochondrial fission and DRP1 activation

(Related to Figure 1)

(A) Left panels, lysates from c-MYC-transduced MEFs for 3.5 days that were incubated during 10 hours with DMSO (as vehicle control) or the MEK1/2 inhibitor PD0325901 (1 µM) were analysed by immunoblotting using the indicated

antibodies. Right graph shows the quantification of ERK1/2 or DRP1 phosphorylation ratios in cells treated with either DMSO (black bars) or PD0325901 (yellow bars).

(B) C-MYC-transduced cells for 3.5 days were incubated with DMSO (as vehicle control) or the PD0325901 (1 μM) for 10 hours. Then, cells fixed and mitochondrial morphology assessed by immunofluorescence. Right panels, representative confocal images of MEFs stained with anti-TOM20 antibody (red). Inset shows a black and white magnification of the pictures. DAPI (blue) was used as a nuclear counterstaining. Graph on the left shows the quantification of the different mitochondrial morphologies observed.

(C) Left panels show representative confocal images of MEFs expressing c-MYC, together with DRP1 wild type (DRP1^{WT}) or the phosphomimetic S579D mutation (DRP1^{S579D}), during 3.5 days. Cells were then treated, fixed and stained as in (C). DAPI (blue) was used as a nuclear counterstaining. Graph on the right shows the quantification of the indicated mitochondrial morphologies observed in the cells transduced and treated as indicated.

(D) Total RNA was extracted from OSKM, OSK or c-MYC-transduced cells at indicated days. Then, *Dusp3*, *Dusp4*, *Dusp5*, *Dusp6*, *Dusp7*, *Dusp9*, *Dusp14* or *Dusp23* gene expression was quantified by qPCR and represented as relative gene expression normalized to control MEFs (n = 3; each independent experiment was conducted in triplicate). Error bars are omitted from the graph for clarity.

Data represent mean ± SEM, one-tailed unpaired t-test (n = 3), * $P < 0.05$, ** $P < 0.01$, *** $P < 0.001$; **** $P < 0.0001$. Scale bars in (B) and (C) are 24 μm.

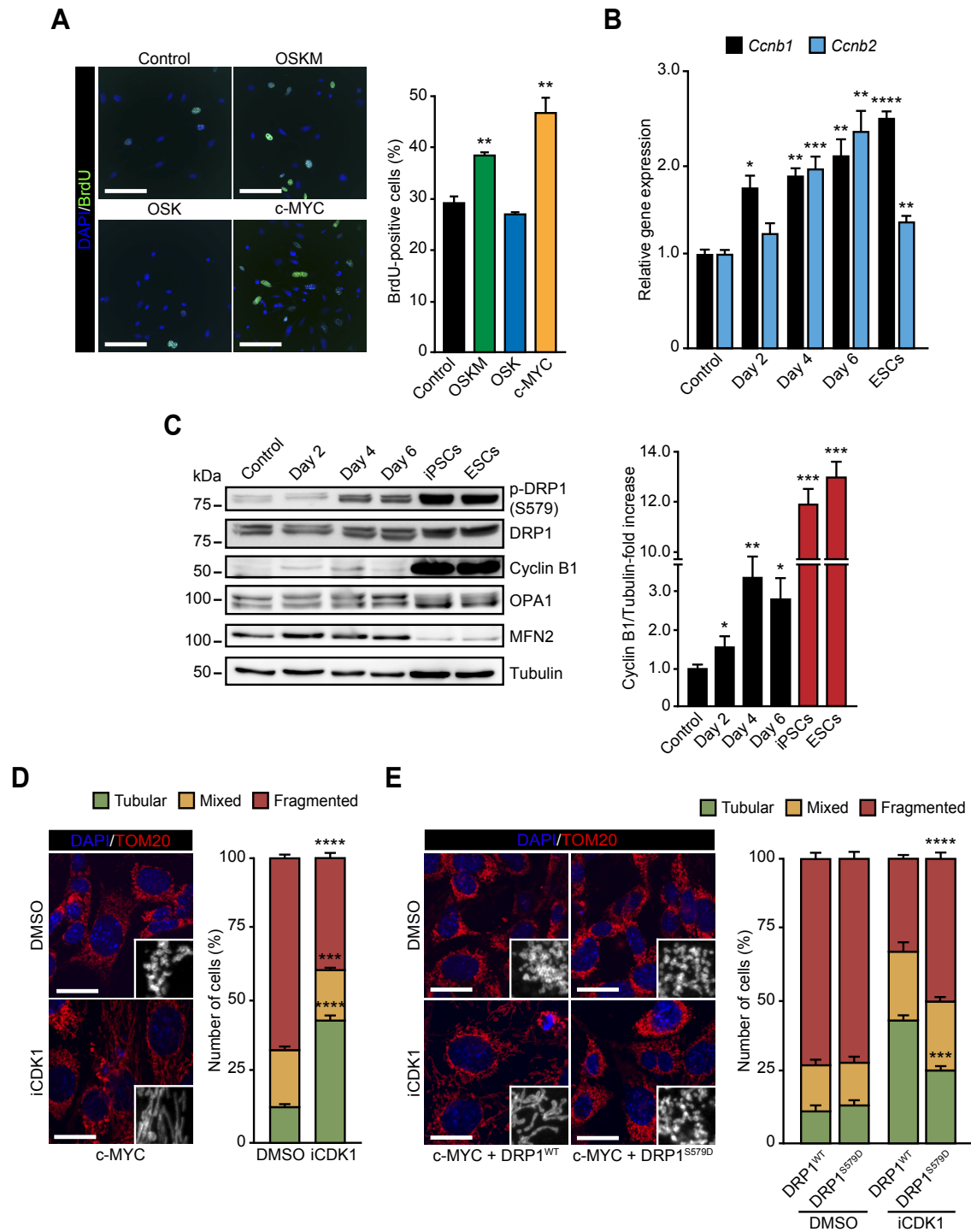**Figure S2. C-MYC induced proliferation early in cell reprogramming**

(Related to Figure 2)

(A) MEFs were mock-infected (control) or transduced with the indicated factors. At day 4 post-transduction, cells were pulsed with 5-bromo-2'-deoxyuridine (BrdU) for 10 minutes, fixed and processed for immunofluorescence with anti-BrdU antibodies (green) and analysed by High-Content microscopy. Left panel,

representative immunofluorescence images (scale bars, 40 µm). Graph on the right shows the quantification of the data.

(B) Total RNA was extracted from MEFs left untreated (control) or OSKM-infected for the indicated days. *Ccnb1* (*Cyclin B1*, black bars) or *Ccnb2* (*Cyclin B2*, blue bars) gene expression was then assessed by qPCR and represented as relative gene expression normalized to control MEFs.

(C) Lysates of MEFs control or expressing OSKM for the specified days were analysed by immunoblotting using the displayed antibodies. Graphs on the right show the quantification of the data corresponding to Cyclin B1 protein expression.

(D) c-MYC-transduced cells for 3.5 days were incubated with DMSO (as vehicle control) or the CDK1 inhibitor RO-3306 (1 µM) for 10 hours (iCDK1). Cells were then treated, fixed and stained as in (Figure S1C). Graph on the right shows the quantification of the indicated mitochondrial morphologies observed in the cells transduced and treated as indicated.

(E) Left panels show representative confocal images of MEFs expressing c-MYC, together with DRP1 wild type (DRP1^{WT}) or the phosphomimetic S579D mutation (DRP1^{S579D}), during 3.5 days. Cells were then treated, fixed and stained as in (Figure S1C). Graph on the right shows the quantification of the indicated mitochondrial morphologies observed in the cells transduced and treated as indicated.

Data represent mean ± SEM, one-tailed unpaired t-test (n = 3), * $P < 0.05$, ** $P < 0.01$, *** $P < 0.001$; **** $P < 0.0001$. Scale bars in (A) 40 µm, in (D) and (E) 24 µm.
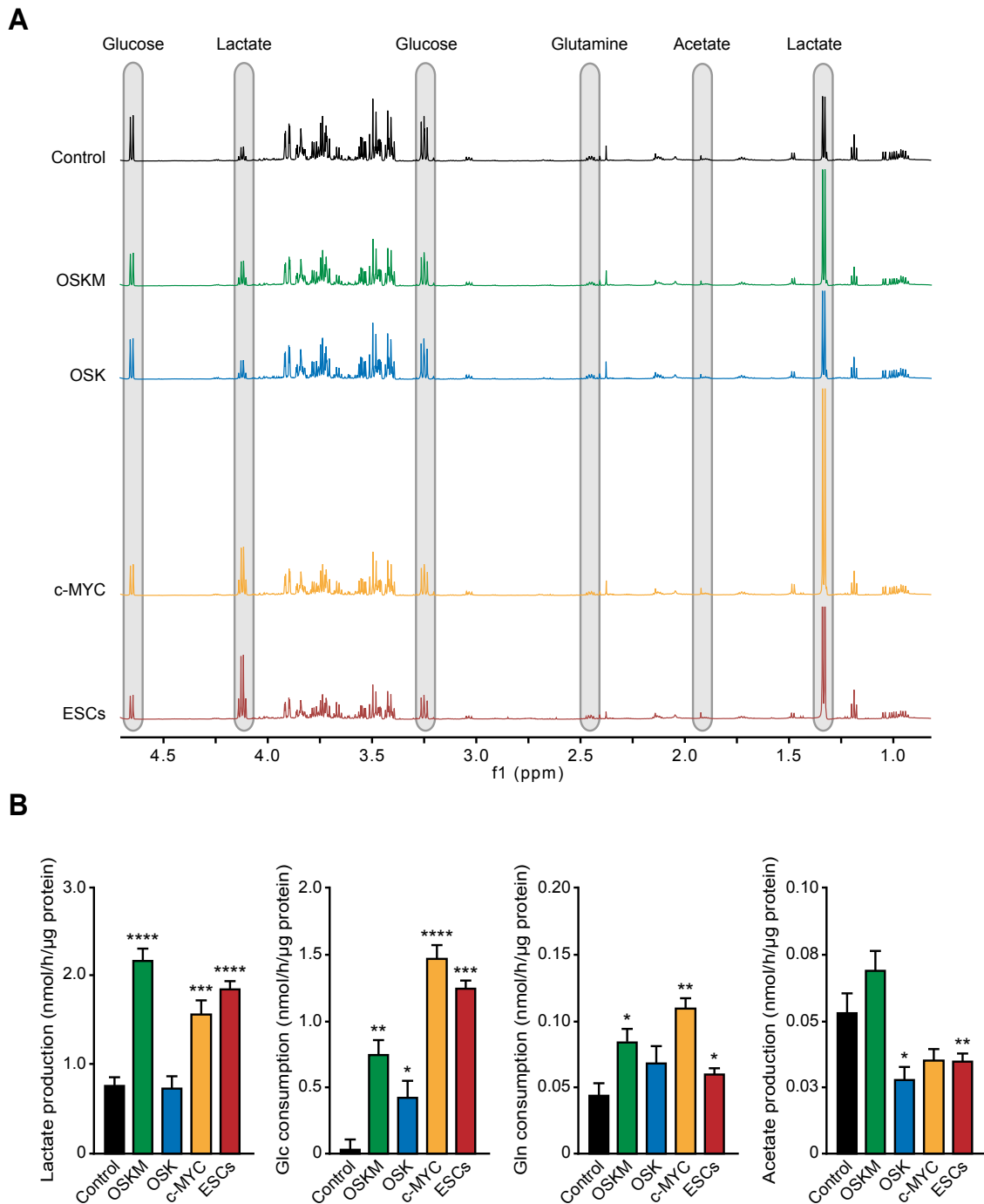
Figure S3. Induction of glycolysis by c-MYC early in cell reprogramming

(Related to Figure 3)

(A) Culture medium from MEFs mock-infected (control) or transduced with the indicated factors was changed at day 2.5 post-transduction. Thereafter, aliquots of conditioned media were taken at 10 (d3), 24 (d4), 48 (d5) or 72 (d6) hours and analyzed by NMR. Diagrams depict metabolomic footprints showing the ^{1}H NMR spectra of the indicated extracellular metabolites acquired at 500 MHz and 27 °C, at day 4 post-transduction with the factors specified on the left.

(B) Bars diagrams showing the kinetics of the metabolites shown in MEFs transduced with the indicated factors for four days, as assessed by NMR.

Data represent mean ± SEM, one-tailed unpaired t-test (n = 3), * $P < 0.05$; ** $P < 0.01$; *** $P < 0.001$; **** $P < 0.0001$.
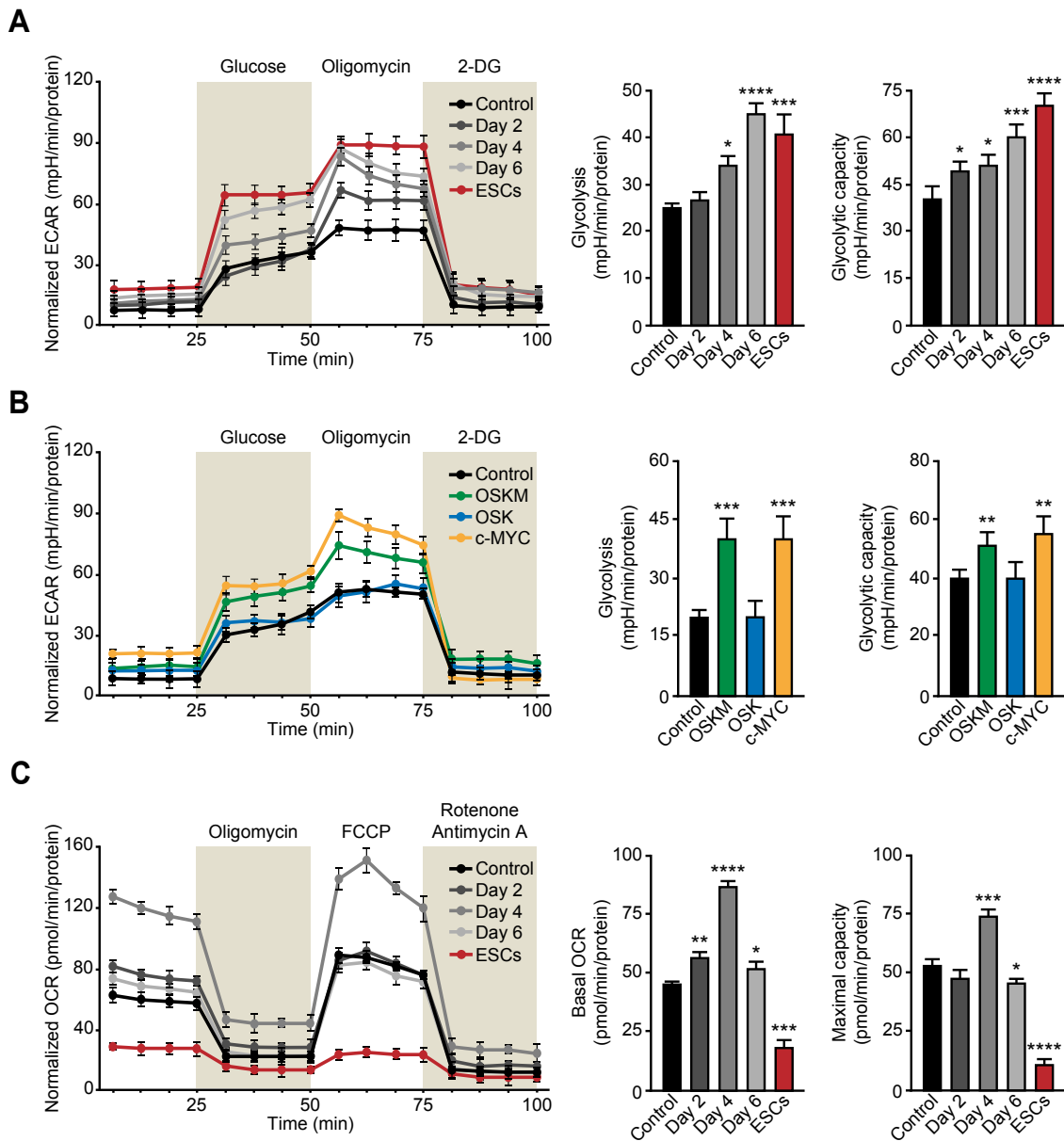
Figure S4. Metabolic profiles during early cell reprogramming

(Related to Figure 3)

(A) Graphs displaying representative extracellular acidification rate (ECAR) in ES cells (ESCs), or in control or OSKM-transduced MEFs for the indicated days.

(B) Graphs displaying representative extracellular acidification rate (ECAR) in MEFs control or transduced with the indicated factors at day 4 post-transduction.

(C) Graphs displaying representative Oxygen Consumption rates (OCR) in ES cells (ESCs), or in control or OSKM-transduced MEFs for the indicated days.

Data represent mean ± SEM, one-tailed unpaired t-test (n = 3, conducted in triplicate), * $P < 0.05$; ** $P < 0.01$; *** $P < 0.001$; **** $P < 0.0001$. FCCP, Carbonyl cyanide-4-(trifluoromethoxy) phenylhydrazone. 2-DG, 2-Deoxy-D-glucose.
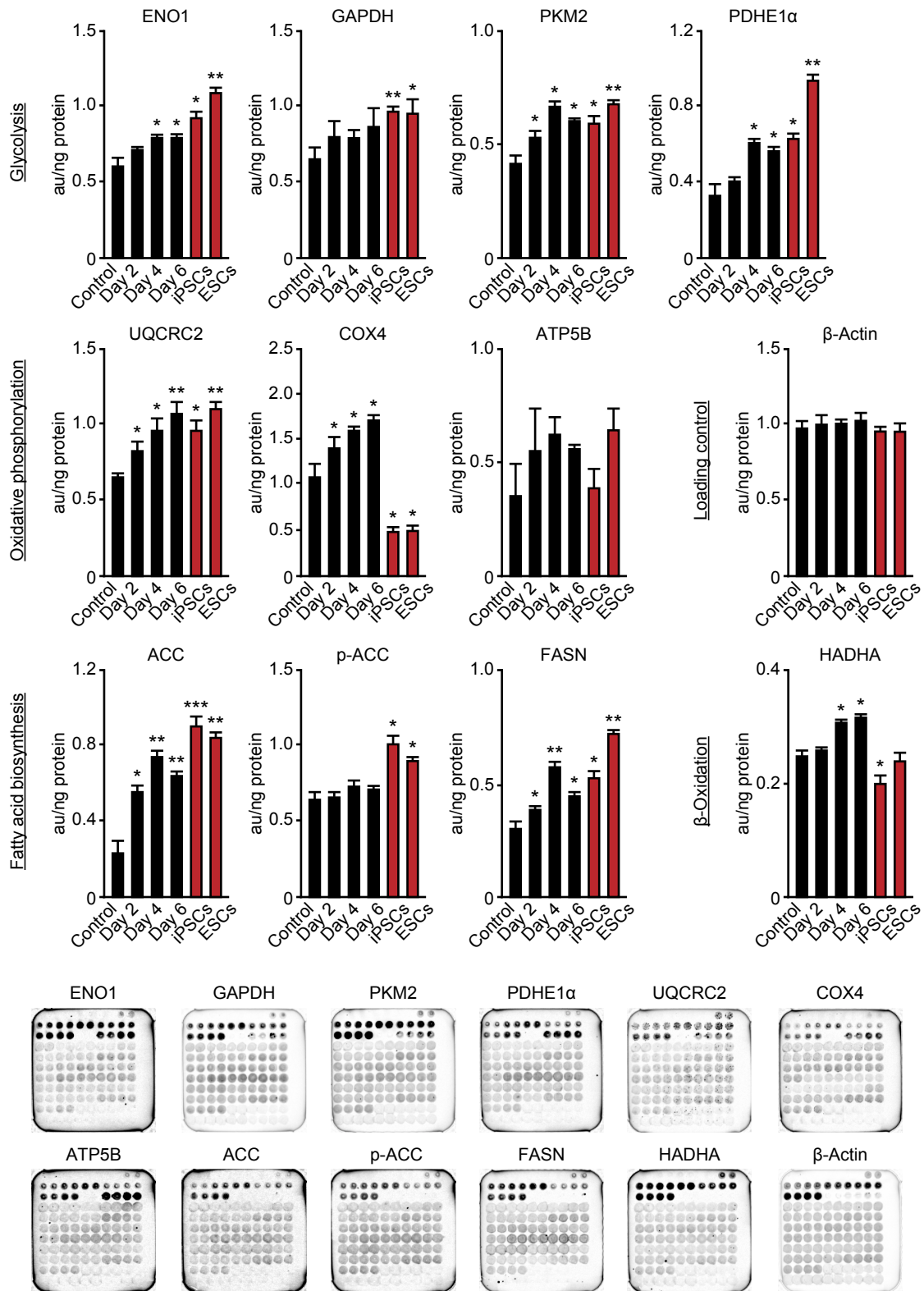
Figure S5. Reverse phase protein antibody microarray analysis of metabolic enzymes during early cell reprogramming

(Related to Figure 4)

Lysates of iPS (iPSCs) or ES (ESCs) cells, MEFs control or transduced with OSKM for the indicated days were analyzed using reverse phase protein arrays. Graphs show the quantification of the data that are represented as mean ± SEM. Bottom panels, representative images from the corresponding protein array pads.

Data represent mean ± SEM, one-tailed unpaired t-test (n = 3), * P < 0.05; ** P < 0.01, *** P < 0.001.
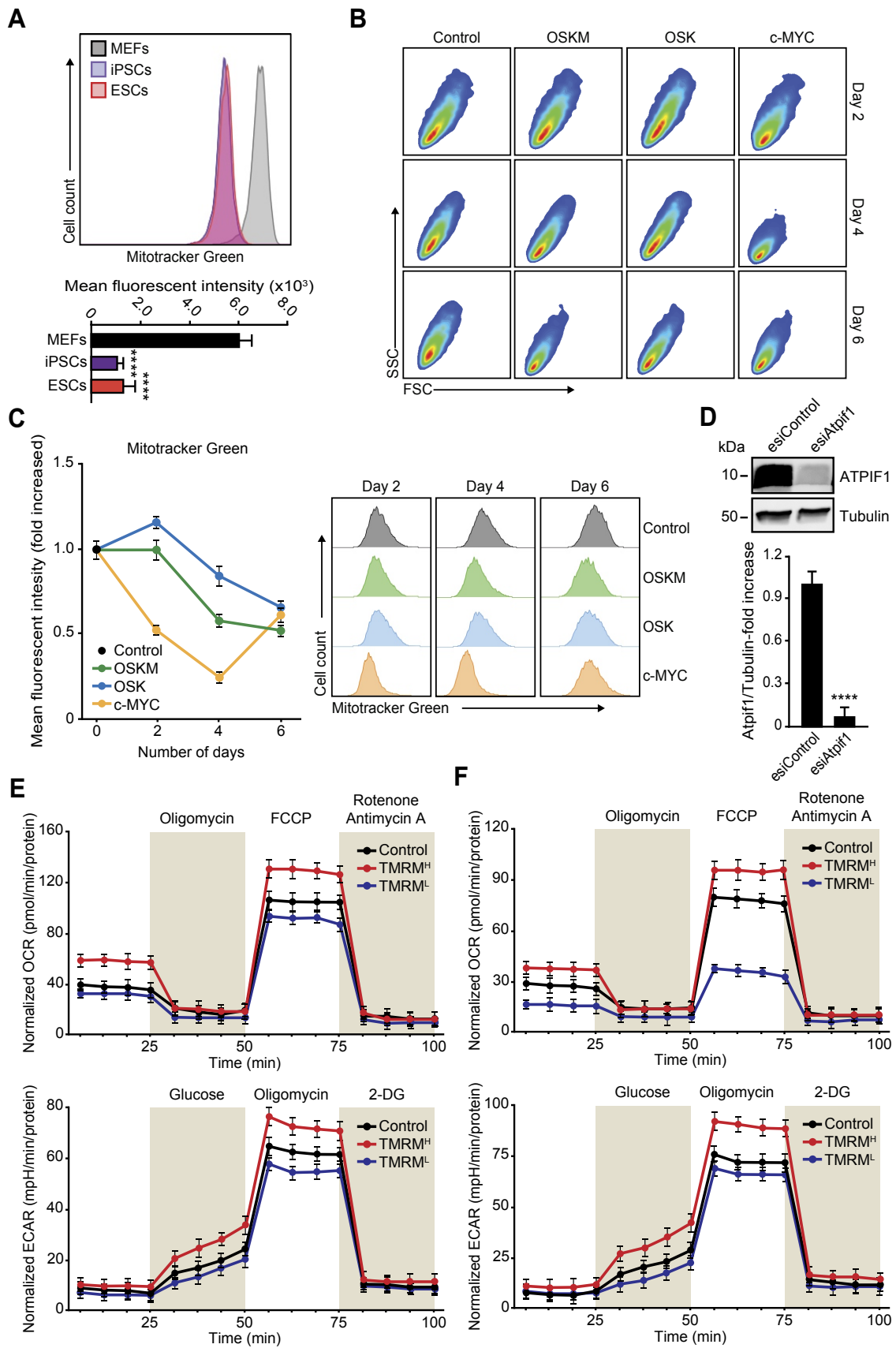
Figure S6. C-MYC increases mitochondrial membrane potential during cell reprogramming

(Related to Figures 5 and 6)

(A) Representative flow cytometry histograms of MEFs, iPS (iPSCs) and ES (ESCs) cells stained with Mitotracker Green FM, a mitochondrial membrane potential-independent probe, to assess mitochondrial mass. Graph underneath shows the quantification of the Mean Fluorescence Intensity of the histograms shown above.

(B-C) Representative flow cytometry histograms of non-transduced MEFs (Control) or transduced with OSKM, OSK or c-MYC-encoding retroviruses and stained with Mitotracker Green FM at the indicated days post-transduction for assessing Forward and Side scatter distributions (B) and mitochondrial mass (C). Graph on the left shows the quantification of the Mean Fluorescence Intensity of the histograms shown in (C).

(D) MEFs transduced with OSKM factors were transfected with esiRNAs targeting either e*GFP* (Control) or *Atpif1* at day 1 post-transduction. At day 6 post-transduction with OSKM retroviruses total lysates were analysed by immunoblotting using the indicated antibodies (upper panels). Graph underneath shows the quantification of the data.

(E-F) Graphs displaying representative oxygen consumption rate (OCR, upper graphs) or extracellular acidification rate (ECAR, bottom graphs) of OSKM-expressing cells sorted based on their TMRM staining intensity at day 6 (E) or 12 (F) post-transduction.

Data represent mean ± SEM, one-tailed unpaired t-test (n = 3), **** $P < 0.0001$. FCCP, Carbonyl cyanide-4-(trifluoromethoxy) phenylhydrazone. 2-DG, 2-Deoxy-D-glucose.

SUPPLEMENTAL EXPERIMENTAL PROCEDURES

Cell culture, reprogramming assays, reagents and plasmids

PlatE (Morita et al., 2000) and SNL (McMahon and Bradley, 1990) cells were grown in high glucose DMEM containing 10% heat-inactivated FBS. When indicated, SNL cells were mitotically inactivated by treatment with 10 μg/ml Mitomycin-C (Sigma-Aldrich) for 2.5 h at 37 °C.

Ecotropic retroviruses were produced in PlatE cells transfected using Polyethylenimine (PEI) "Max" (Mw 40,000) (Polysciences) exactly as described (Takahashi and Yamanaka, 2006; Prieto et al., 2016a; Prieto et al., 2016b). For cell reprogramming, 8×10^5 MEFs were plated per p100 mm the day before the assay. Next day (day 0), MEFs were incubated overnight with a mixture of mouse OCT4, SOX2, KLF4 and c-MYC retroviral supernatants supplemented with 4 μg/ml Polybrene (1:1:1:1 for OSKM, 1:1:1 for OSK and 1:4 for c-MYC). Next day, the supernatants were replaced with fresh media and cells were incubated for 3 more days (day 4). At day 2 media was changed to ES cell culture media containing 15 % FBS and LIF. Media was changed every other day. When indicated, cell reprogramming was conducted in the presence of DMSO (as control), 10 μM of c-MYC inhibitor 10058-F4 (Selleckchem), 10 μM of the CDK1 inhibitor RO-3306 (Merck), 1 μM of the MEK1/2 inhibitor PD0325901 (Millipore) or 0.5 μM Rotenone (Selleckchem). For assessing cell reprogramming efficiency (AP-staining) in the presence or absence of the MYC inhibitor (Figure 1A), OSKM-transduced cells for four days were plated (5×10^4 cells) on a confluent layer of mitotically-inactivated SNL feeders seeded the day before on gelatin-coated p60 mm at $2,5 \times 10^6$ cells per

dish. OSK-transduced cells were not plated on a confluent layer of feeders and were maintained in their original plate without reseeding. At day five post-transduction, MYC inhibitor or vehicle control were added to the plates and renewed every other day until the end of the experiment. AP-staining was performed at day 25.

Westernblot

Signals in western blots were detected using ECL prime (Amersham) and images automatically captured in an Alliance Mini HD9 digital imaging system equipped with a 16-bit (65536 grey levels) scientific grade camera with variable electronic shutter speed and 4.8 OD dynamic range (UVITEC). Acquired images were processed using Adobe Photoshop CS6 and analysed with ImageJ software.

High-content analysis

For the analysis, cells and nuclei were defined using the Hoechst 33258 staining. The nuclei were segmented using top-hat segmentation defining a minimum nucleus area of 50 μm^2. To define the cell segmentation a collar segmentation routine was used, specifying a ratio of 4 μm. To analyse the expression of BrdU by cell, the average intensity of pixels in the reference channel (AlexaFluor-549) within the defined nuclear region was measured. Once each cell had associated a nuclear intensity for the specific expression, a threshold filter defining positive and negative expressing cells was set. Threshold filter uses a histogram for data visualization. To specify the filter settings, the nuclear intensity measurement was selected. The threshold filter defines the cells with nuclear intensities above or below a given value as positive or negative respectively, for the expression of the protein. As a result, the program assigns to each cell the definition of positive or negative for the

expression of BrdU and generates a percentage of both cell populations (positive and negative) per well.

Printing and processing of reverse phase protein arrays

For printing, serially diluted protein extracts (0–1 μg/μl) derived from HCT116 colocarcinoma and BT-549 breast cancer cell lines were also prepared to assess printing quality and the linear response of protein recognition by the antibodies used. A standard curve of BSA (0-1 μg/μl) and mouse IgGs (0-0.6 ng/ml) were also prepared for printing as internal negative and positive controls, respectively. 1 nl volume of each sample was spotted in duplicate onto nitrocellulose-coated glass slides containing 16 pads (FAST Slides, Scheleicher & Schuell BioScience, Inc.) using a BioOdyssey Calligrapher MiniArrayer printer (Bio-Rad) equipped with a solid pin (MCP310S) at constant humidity (RH 45 %) and 10 °C and 16 °C for the plate and chamber, respectively.

After printing, arrays were allowed to dry and further blocked in PBS-T containing 5 % skimmed milk. After, each pad in the array was incubated overnight at 4 °C with the indicated concentrations of highly specific primary monoclonal or polyclonal antibodies. Spotted samples in one of the pads were fixed with XFCF buffer (10% acetic acid, 30% ethanol) for 1h, stained with 0.0001% Fast Green FCF (Sigma-Aldrich) in XFCF for 5 minutes and washed 5 times with XFCF in order to quantify the total protein amount of each spot. The other pads, after incubation with the primary antibodies, were washed with PBS-T and further incubated with a goat anti-mouse highly cross-adsorbed antibody conjugated with CF-647 (Sigma-Aldrich, 1:500) or, in the case of rabbit antibodies, a donkey anti-rabbit secondary antibody

conjugated with alexa-647 (1:500) (Invitrogen). Microarrays were scanned using a Typhoon 9410 scanner (GE Healthcare). The mean fluorescent intensity of the spots was quantified using GenePix Pro 7 software system and converted into arbitrary units of expressed protein per ng of protein in the sample, using the expression obtained in the standard curve of the HCT116 cell line and normalized to the protein amount in the sample obtained from the FCF stained pad. Representative technical variances of the β-Actin arrays, calculated by the squared coefficient of variation (SCV = σ*100/|x|), were 4.8 ± 0.7. Details of the used antibodies are provided in Supplemental Tables 1 and 2.

Metabolomic footprinting

For NMR analysis, 60 μL of D_2O (Eurisotop) containing 5 mM sodium 3-(trimethylsilyl) propionate-2,2,3,3-d4 (TSP) (Eurisotop) for chemical shift reference and 92.50 mM formate (Sigma) for peak quantification, reference was added to 540 μL of medium. The concentration of the formate stock solution was previously calibrated with a quantitative 1D NMR experiment, applying the Eretic Signal (Bruker Biospin). Samples were then centrifuged for 5 min at 10,000 X*g* and the supernatant transferred to 5 mm NMR tubes (DeuteroGmB). ^{1}H NMR analyses were carried out on a Bruker Ultrashield Plus 500 MHz spectrometer with a TBI probe. A NOESY mixing time of 0.01 s was applied for improving the baseline and the water signal was suppressed with pre-saturation. The spectra were acquired over a width of 30 ppm with 96 k data points and an acquisition time of 2.7 s. 64 scans were accumulated for each spectrum and the relaxation delay was set to 4 s. Spectra were processed with an exponential line broadening of 0.5 Hz and a zero filling to 128 k. The baseline was corrected manually and the spectra referenced to

the TSP peak (0.00 ppm) using MestReNova 8.1 software (MestRelab Research). Metabolite assignment was performed with the help of the Human Metabolome database and published literature. Metabolite concentrations in basal media were subtracted from concentrations of metabolites in 10-to-72 h conditioned media for the calculation of net fluxes. The resulting rates were normalized to total cellular protein content determined by a BCA protein assay (Pierce, Thermo-Scientific)

Extracellular metabolic flux analysis

Basal and uncoupled oxygen consumption rates (OCR), or extracellular acidification rates (ECAR), were measured using a Seahorse bioanalizer (XF96) and the Mito or Glycolysis stress test kits (both from Seahorse Bioscience, Millipore), respectively. Cells (20,000-30,000 cells per well) were plated the day before the measurements on XF96 culture microplates. Next day, media was changed to unbuffered XF Base medium supplemented with 2 mM Glutamine (glycolysis stress kit), or 25 mM glucose, 1 mM Sodium Pyruvate and 2 mM Glutamine (mitochondria stress kit) and equilibrated for 1 hour at 37 °C without a CO_2 supply. For OCR assessment, Oligomycin (1 μM), FCCP (1 μM) and Antimycin A/Rotenone (0.5 μM) were used. For ECAR assessment, glucose (10 mM), oligomycin (1 μM) and 2-Deoxy-D-glucose (50 mM) were used. Measurements were taken every 5 minutes after addition of the drugs (a total of 4 readings per reagent added) and results were normalized to the total cellular protein content determined by a BCA protein assay. Each experiment was conducted in triplicate and repeated at least 3 times.

SUPPLEMENTAL REFERENCES

McMahon AP and Bradley A (1990) The Wnt-1 (int-1) proto-oncogene is required for development of a large region of the mouse brain. Cell 62:1073-1085.

Morita S, Kojima T and Kitamura T (2000) Plat-E: an efficient and stable system for transient packaging of retroviruses. Gene Ther 7:1063-1066.

Table S1. Primary antibodies used in this study.

Antigen	Host[a]	Company, reference[b]	Dilution, (application)[c]
ACC	Rb	CST, #3676	1:1000 (WB)
p-ACC (Ser79)	Rb	CST, #11818	1:1000 (WB)
β-Actin	Ms	SA, A2547	1:500 (PMA)
ATP5B	Ms	In house (J.M. Cuezva)	1:150 (PMA)
ATPIF1	Rb	SCBT, sc-134962	1:500 (WB)
BrdU	Rt	ID, OBT0030	1:500 (IF/HCA)
Cyclin B1	Ms	SCBT, sc-245	1:100 (WB)
COX4	Ms	Abcam, ab14744	1:100 (PMA)
DRP1	Rb	CST, #8570	1:1000 (WB); 1:50 (IF)
p-DRP1 (Ser616)	Rb	CST, #3455	1:1000 (WB)
ENO1	Rb	Abgent, AM2192b-ev	1:200 (PMA)
ERK1/2	Rb	CST, #9102	1:1000 (WB)
p-ERK1/2 (Thr202/Tyr204)	Ms	CST, #9106	1:2000 (WB)
FASN	Rb	CST, #3180	1:1000 (WB)
GAPDH	Rb	CST, #5174	1:1000 (WB)
GAPDH	Ms	In house (J.M. Cuezva)	1:250 (PMA)
HADHA	Rb	Abcam, ab54477	1:1000 (PMA)
HK1	Rb	CST, #2024	1:1000 (WB)
HK2	Rb	CST, #2867	1:1000 (WB)
LDHA	Rb	CST, #3582	1:1000 (WB)
MFN2	Rb	SA, AV42420	1:1000 (WB)
NDUFS3	Ms	SCBT, sc-374282	1:200 (IF)
OPA1	Ms	BD, #612606	1:1000 (WB)
PDH	Rb	CST, #3205	1:1000 (WB)

PDHE1α	Ms	TFS, 459400	1:200 (PMA)
PKM1/2	Rb	CST, #3190	1:1000 (WB)
PKM2	Ms	In house (J.M. Cuezva)	1:150 (PMA)
SDHA	Rb	SCBT, sc-11998	1:300 (WB)
TOM20	Rb	SCBT, sc-11415	1:50 (IF); 1:500 (WB)
TOM20	Ms	SA, WH0009804M1	1:500 (IF)
α−Tubulin	Ms	SCBT, sc-32293	1:5000 (WB)
UQCRC2	Ms	Abcam, ab14745	1:500 (PMA)

(*a*) Rb, rabbit; Ms, Mouse, Rt, Rat.

(*b*) SCBT, Santa Cruz Biotechnology; CST, Cell Signaling Technologies; ID, Immunological Direct; SA, Sigma-Aldrich; BD, BD Biosciences.

(*c*) IF, immunofluorescence; HCA, High-Content analysis; PMA, reverse phase protein microarrays; WB, Western blot.

Table S2. Secondary antibodies used in this study.

Antigen	Host[a]	Conjugated[b]	Company, reference[c]	Dilution, (application)[d]
Mouse IgG	Dk	AF–488	TFS, A-21202	1:1000 (IF)
Mouse IgG	Dk	AF–555	TFS, A-31570	1:1000 (IF)
Mouse IgG	Dk	AF–647	TFS, A-31571	1:1000 (IF)
Mouse IgM	Dk	AF–555	TFS, A-21426	1:1000 (IF)
Rabbit IgG	Dk	AF–488	TFS, A-21206	1:1000 (IF)
Rabbit IgG	Dk	AF–555	TFS, A-31572	1:1000 (IF)
Rabbit IgG	Dk	AF–647	TFS, A-31573	1:1000 (IF)
Rat IgG	Dk	AF–488	TFS, A-11006	1:1000 (IF)
Mouse IgG	Gt	HRP	TFS, 31432	1:5000 (WB)
Rabbit IgG	Gt	HRP	TFS, 31460	1:5000 (WB)
Mouse IgG	Gt	CF–647	SA, SAB4600183	1:500 (PMA)
Rabbit IgG	Dk	AF–647	TFS, A-31573	1:500 (PMA)

(*a*) Dk, donkey; Gt, goat.

(*b*) AF, AlexaFluor; CF, cyanine-based fluorescent dye; HRP, Horseradish Peroxidase

(*c*) SA, Sigma-Aldrich; TFS, Thermo Fisher Scientific.

(*d*) FC, flow cytometry; IF, Immunofluorescence; PMA, reverse phase protein microarrays; WB, Western blot.

Table S3. Sequences of the primers used in this study for qPCR analysis employing SYBR Green.

Gene	Forward primer (5' to 3')	Reverse primer (5' to 3')
Atpif1	*ACCATTCGAAGGAGATAGAG*	*ATTCAAAGCCATGTGTCTAC*
Ccnb1	*ACATGACTGTCAAGAACAAG*	*CAGATGTAGCAGTCTATTGG*
Ccnb2	*GCCAAGGAAAATGGAATTTG*	*TACGGTTGTCATTGACTTTC*
Dusp3	*CACCACAAACCAAAAACATC*	*CATGCTATCCTTGACCTTTC*
Dusp4	*TATTGAGTGGAGAGGGAAAG*	*ATTCCTGTGAGTTCAACAAC*
Dusp5	*AAATCCTTCCCTTCCTCTAC*	*CTTGAAAGTGGGAGCTAATG*
Dusp6	*ATGATGAGGTCTTCAGTCTC*	*CAAAATACCCCTTGAGACAC*
Dusp7	*GAGAGAGAGAGTGTTCTCAG*	*AGGTAGGAAATGGTAGAACC*
Dusp9	*CGTCTGTGACTGTTACTTTC*	*TGTGGCAAAGAATGATACAC*
Dusp14	*CATCATCCCAGACGTTTATG*	*CATCTCTTAAACCCGAACAC*
Dusp23	*CATTGAGACGTATGAACAGG*	*AGTACTTTAGTTCACTCCCC*